Universidade de Aveiro

2021

Maria Araújo Medeiros

Materiais inorgânicos minimalistas obtidos através de impressão 3D

Minimalistic inorganic based approaches towards 3D printed biomaterials

Universidade de Aveiro

2021

Maria Araújo Medeiros

Materiais inorgânicos minimalistas obtidos através de impressão 3D

Minimalistic inorganic based approaches towards 3D printed biomaterials

Dissertação apresentada à Universidade de Aveiro e ao Departamento de Física da mesma instituição para cumprimento dos requisitos necessários à obtenção do grau de Mestre em Engenharia Biomédica, realizada sob a orientação científica do Doutor Tiago Ruivo Correia, Investigador Júnior do Departamento de Química da Universidade de Aveiro e do Professor Doutor João Filipe Colardelle da Luz Mano, Professor Catedrático do Departamento de Química da Universidade de Aveiro.

Dissertation presented to the University of Aveiro and to the Department of Physics of the same institution to fulfil the necessary requirements to obtain the Master of Science Degree in Biomedical Engineering, carried out under the scientific supervision of Doctor Tiago Ruivo Correia, Junior Researcher at Department of Chemistry of University of Aveiro, and Professor Doctor João Filipe Colardelle da Luz Mano, Cathedratic Professor of the Department of Chemistry at University of Aveiro.

This thesis was financially supported by national funds (OE) through FCT/MCTES in the scope of the following project:

COP2P (PTDC/QUI-QOR/30771/2017), which was also supported by FEDER through the "Programa Operacional Competividade e Internacionalização" (POCI-01-0145-FEDER-030771).

À minha família, por todo o apoio e pelo objetivo que me ajudaram a alcançar.

To my family, for all the support and the goal they helped me to reach.

Agradecimentos

Esta tese de mestrado apresenta-se como o marco final de uma incrível jornada académica e, apesar de ser um trabalho individual, não poderia deixar de frisar a importância de toda a ajuda e apoio que me foi cedido para a realização deste trabalho. Assim, gostaria de agradecer formalmente algumas pessoas que levarei em consideração ao longo da minha vida.

Em primeiro lugar, gostaria de agradecer ao professor João Mano pela oportunidade de trabalhar no COMPASS, um grupo de investigação que prima pela excelência e inovação. Foi um grande desafio, mas sem dúvida que foi uma experiência muito enriquecedora, tanto a nível pessoal como profissional.

Um agradecimento especial ao Dr. Tiago Correia, o meu orientador, por toda a sua disponibilidade e orientação durante este percurso, permitindo-me sempre todos os recursos necessários para a realização desta tese. Obrigada por teres acreditado em mim e no trabalho que fomos desenvolvendo.

Não posso deixar de agradecer a todo o elenco do grupo COMPASS, que de uma forma ou outra contribuíram para conclusão deste capítulo. Em especial ao Dr. João Rodrigues, à Marta Maciel e ao Edgar Castanheira por toda a disponibilidade e ajuda durante o trabalho de laboratório, e por tudo o que me ensinaram ao longo deste ano. Ao Paulo e à Ana, por se mostrarem sempre disponíveis a ajudar-me no que fosse preciso e pela ajuda na adaptação inicial ao laboratório.

Aos amigos que fiz no curso, por todo o companheirismo, apoio e momentos de diversão ao longo destes 5 anos. Tornaram este percurso mais fácil.

Ao Leandro, por todo o carinho, motivação e força que partilha diariamente comigo, pela companhia ao longo de todo este grande e desafiante percurso.

Por último, tendo consciência que sem eles nada disto seria possível, dirijo o meu maior obrigada aos meus pais, pelo apoio incondicional, incentivo e paciência demonstrados não só no decorrer desta tese, mas em todos os momentos da minha vida. Obrigada por me terem ensinado sempre a superar todos os obstáculos e por me permitirem ser quem sou hoje. Vocês são o meu maior exemplo.

o júri

Presidente	Prof. Doutora Ana Luísa Monteiro da Silva Professora Auxiliar em Regime Laboral, Universidade de Aveiro
Vogal- Arguente principal	Prof. Doutor André Ferreira Moreira Professor Auxiliar Convidado, Universidade da Beira Interior
Vogal - Orientador	Doutor Tiago Ruivo Correia Investigador Doutorado (nível 1), Universidade de Aveiro

palavras-chave

Híbridos, Superfícies de Energia Mínima, 3D printing, Engenharia de Tecidos

resumo

Com o aparecimento da tecnologia de fabricação aditiva (FA) em meados dos anos 80, muitas aplicações beneficiaram de um processamento mais rápido dos produtos sem a necessidade de ferramentas específicas. Contudo, a utilização das tecnologias de FA na Engenharia de Tecidos (ET) com destino à aplicação óssea tem vindo a crescer nos últimos anos. Entre as diferentes opções tecnológicas, a impressão tridimensional (3DP) está a tornar-se popular devido à capacidade de produzir *scaffolds* porosos com geometria definida e porosidade interligada. Tendo como fonte de inspiração os filmes de sabão, uma forma promissora e inovadora de conceber novos biomateriais com características únicas baseadas na geometria de energia mínima de vários modelos tridimensionais (3D) impressos foi pela primeira vez estudada. Desta forma, o trabalho de tese aqui apresentado centra-se na fabricação de *scaffolds* com base na tensão superficial formada após a imersão de geometrias numa solução de tensioativos. Como substituto dos tensioativos sintéticos, o quitosano (CH), um polímero catiónico derivado de crustáceos marinhos, foi utilizado e modificado com grupos metacrílicos (MA) a fim de ser foto reticulado quando misturado com um fotoiniciador (LAP). A modificação do quitosano foi confirmada pela técnica de caracterização ^{1}H NMR e ATR-FTIR. Paralelamente, a solução precursora de sílica (TEOS) preparada pelo método de sol-gel foi posteriormente adicionada à solução de quitosano metacrilado, obtendo-se assim uma solução híbrida composta por fases orgânica e inorgânica. Os filmes híbridos foram produzidos através da imersão dos modelos geométricos 3D na solução híbrida e subsequente foto reticulação. Diferentes formulações de soluções híbridas (com diferentes quantidades de composto inorgânico) foram avaliadas através das técnicas de microscopia eletrónica de varrimento (SEM) e espectroscopia de raios X (EDS). De forma a complementar a caracterização das estruturas híbridas, estas foram também analisadas recorrendo à microscopia de fluorescência para verificar a distribuição da componente inorgânica por todo o *scaffold*. Verificou-se ainda que a combinação de um composto inorgânico com um de carácter orgânico, melhora o comportamento de decomposição térmica. Como prova de conceito, foram efetuados estudos *in vitro* sendo que, os *scaffolds* híbridos produzidos neste trabalho não demonstraram capacidade para formar cristais de hidroxiapatita quando imersos em SBF (Simulação de Fluidos Corporais), contudo, apresentaram um perfil biocompatível quando em contacto com uma linha celular standard.

keywords Hybrids, Minimal Surfaces, 3D printing, Tissue Engineering

abstract

With the advent of additive manufacturing (AM) technologies in the mid-1980s, many applications benefited from the faster processing of products without the need for specific tooling. However, the use of AM technologies in bone tissue engineering has been growing in recent years. Among the different technology options, three-dimensional printing (3DP) is becoming popular due to the ability to produce porous scaffolds with designed shape and interconnected porosity. Taking soap films as a source of inspiration, a promising and novel way of designing new materials with unique features based on minimum energy geometry of 3D printed models has been studied for the first time. Thus, the thesis work here presented focuses on fabrication of scaffolds based on the surface tension formed after immersing geometries in a surfactant solution. As a substitute for synthetic surfactants, chitosan (CH), a cationic polymer derived form marine crustaceans was used and modified with methacrylic groups (MA) in order to be light cured when mixed with a photoinitiator (LAP). The chitosan modification was confirmed by ^{1}H NMR and ATR-FTIR characterization techniques. In parallel, the silica precursor (TEOS) solution prepared by sol-gel chemistry was subsequently added to the methacrylated chitosan solution, thus obtaining a hybrid solution composed of organic and inorganic phases. The hybrid films were produced by immersing the 3D geometric models into the hybrid solution and subsequent photo- crosslinking. Different formulations of hybrid solutions (with different amounts of inorganic compound) were evaluated using scanning electron microscopy (SEM) and X-ray photoelectron spectroscopy (EDS) techniques. In order to complement the characterization of the hybrid structures, they were also analyzed using fluorescence microscopy to verify the distribution of the inorganic component throughout the scaffold. It was also verified that the combination of an inorganic compound with an organic one improves the thermal decomposition behavior. As proof of concept, in vitro studies were carried out and the hybrid scaffolds produced in this work did not demonstrate the ability to form hydroxyapatite crystals on its surface when immersed in Simulated Body Fluid (SBF), however, presents a biocompatible profile when in contact with a standard cell line.

CONTENT

List of figures

List of tables

List of Abbreviations and Acronyms

2D	Bi-dimensional
3D	Three-dimensional
^{1}H NMR	Proton Nuclear Magnetic Resonance
ATR-FTIR	Attenuated Total Reflectance Fourier Transformed Infrared
CMC	Critical Micelle Concentration
CH	Chitosan
CH-MA	Methacrylated Chitosan
D_2O	Deuterium Oxide
DMEM-LG	Dulbecco's Modified Eagle Medium – Low Glucose
DPBS	Dulbecco's phosphate-buffered saline
DS	Degree of substitution
DW	Distilled Water
EDS	Energy Dispersive X-Ray Spectroscopy
FBS	Fetal bovine serum
FITC	Fluorescein isothiocyanate
LAP	Lithium phenyl-2,4,6-trimethylbenzoylphosphinate
LMWC	Low Molecular Weight Chitosan
MA	Methacrylic Anhydride
PBS	Phosphate-buffered saline
PI	Propidium iodide
RT	Room temperature
SBF	Simulated body fluid
SEM	Scanning Electron Microscopy
TE	Tissue Engineering
TGA	Thermogravimetric analysis
UV	Ultraviolet

1. Motivation

Throughout their lives, humans may suffer from some diseases or traumas that consequently cause dysfunctions in the affected tissues/organs, as well as the proper functionality of their metabolism. Thus, alternatives to traditional treatments such as repairing surgeries, organ transplantation, etc., have been studied because in the latter case these are processes limited in their applicability due to the compatibility of allografts and the disparity between the number of organs and tissues required and the number available for clinical applications [1]. Additionally, they often cannot achieve the full repair of the damage tissue and, therefore, require painful surgical procedures. Tissue engineering (TE) is a multidisciplinary field that emerged with the aim of creating biomaterials that mimic the morphology and physiological, biological, chemical and mechanical properties of the original tissues to promote tissue growth and regeneration [2], [3] controlling the entire biological environment. Tissue regeneration in adults focuses on reviewing developmental processes and focuses on maintaining, or restoring, the integrity of the tissue and its functionality [3]. It is an area that covers a wide range of applications with the purpose of repairing or replacing parts of whole tissues or tissues, such as bone, cartilage, blood vessels, skin and muscle [2].

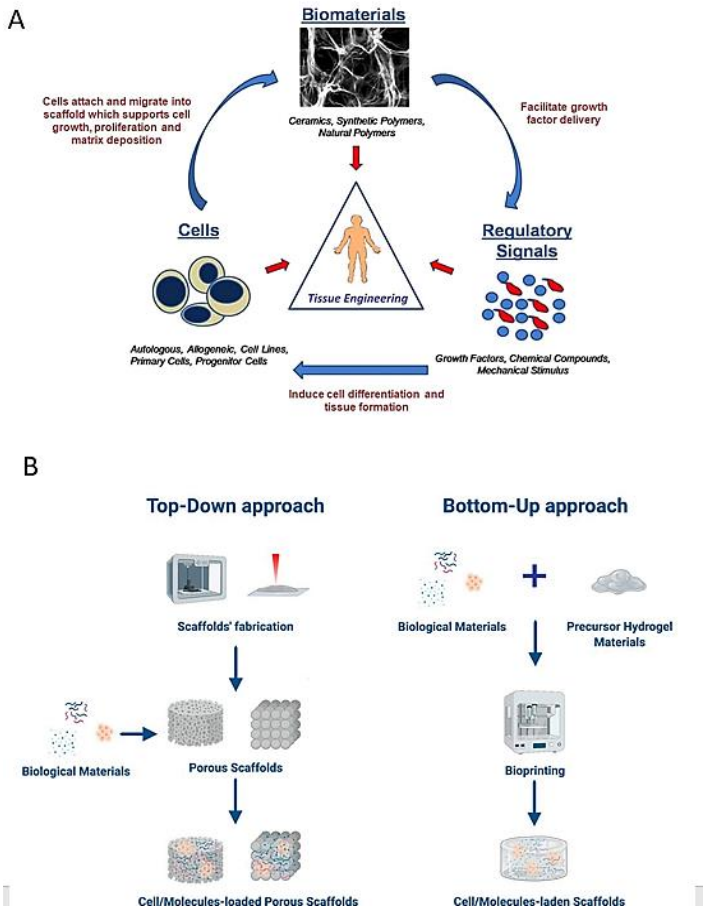

Figure 1. (A) Tissue engineering (TE) triad. The interaction of biomaterials, regulatory signals and cells enables the production of biomaterials in TE field. Reproduced from [5]; (B) Schematization of the approaches applied in additive manufacturing (AM) techniques. Reproduced from [7].

TE focuses primarily on the permanent healing and adopts different approaches individually or in combination: cell-based therapies, growth factors that induce tissue formation and the delivery of cells through biocompatible structures [4]. This last concept is closer to the concept of TE based on the use of living cells within a natural or synthetic substrate - scaffold - that mimics the extracellular matrix (ECM). The biomaterial system may include the scaffold – that provides structure and substrate for tissue growth and development, cells – to help the formation of target tissue and growth factors, cytokines, and other biological agents that could mimic the biochemical microenvironment and stimulate and guide the process of tissue regeneration – Figure 1-A [5].

TE is mainly based on two approaches: Top-down or bottom-up (Figure 1-B). Top-down approach employs additive manufacturing (AM) techniques to produce 3D scaffolds with the desired architecture to guide the formation of the target tissue. Here, living cells are seeded on or within the porous 3D structures. The major advantages of this strategy are the possibility to use a wide range of materials, ranging from ceramics to polymers and hydrogels, and the possibility of producing porous scaffolds with specific mechanical properties depending on the application of interest [6]. On other hand, the lack of proper vascularization of the construct and the cell seeding into porous is also inefficient due to the ability of cells to penetrate the central part of the scaffold represents some limitations of this approach. In the bottom-up approach, scaffolding materials, cells, and sometimes also bioactive compounds are assembled together to give rise to scaffolds of several shapes and sizes. This approach has been gaining more and more relevance because they allow for a good control over the spatial arrangement of cells, obtaining an architecture that could mimic the assembly of native tissue [7], [8]. Some disadvantages are the low mechanical properties and the low speed of fabrication [6], [7].

In this field, the physical and biochemical characteristics of the scaffold are important since these may have a considerable effect on cell differentiation [9]. Features of scaffolds such as stiffness mechanics, surface topography and functional chemical groups can be modulated to give rise to a specific tissue line [3]. It is reported in the literature that the geometry of scaffolds used in tissue engineering determines the magnitude of the cellular response and thus, the rate of regeneration of the target tissue. The tissue regeneration increases with the curvature of the surface, thus preferring concave to convex surfaces [10]. Additive manufacturing (AM), also called as three dimensional (3D) printing or rapid prototyping, is a technology which has been widely used in the TE area. It allows to design materials with high precision, controlled geometry and architecture, appropriate curvature and porosity depending on their application [10].

Minimal surfaces are surfaces which the curvature along the principal curvature planes are equal and opposite at every point, which means that their mean curvature is zero [11]. The images present in Figure 2 shows the minimum surface area of the various geometric shapes that are represented below. What happens is that when the structure is removed from a soap solution, the soap film configuration created is given by the smallest area of that structure, in order to reach equilibrium [12]. Just as the soap film tries to minimize its energy, a thermodynamic system tends to that state where free energy is minimal [12], [13].

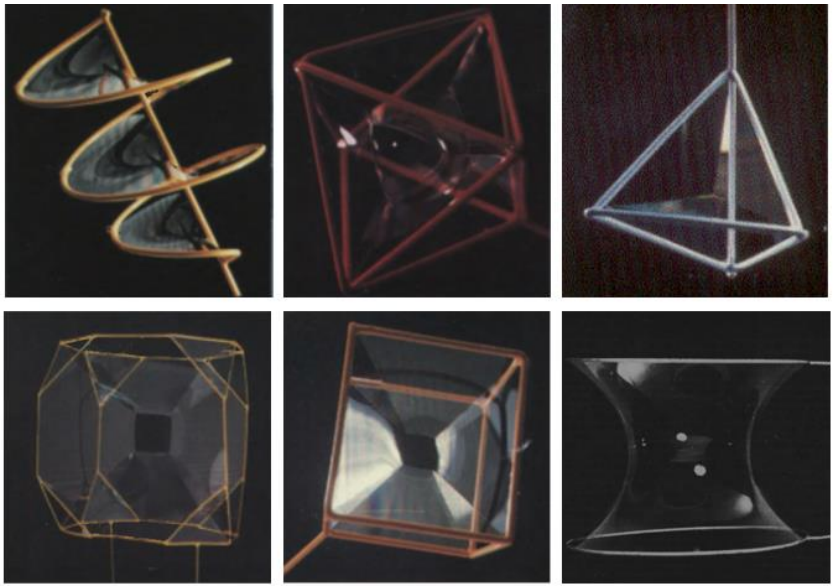

Figure 2. Minimal surfaces defined by soap films. The geometries shown are (from top left to bottom right) helix with a central axis, octahedron, tetrahedron, truncated cube, square and catenoid. Adapted from [12].

This type of structures design is so appreciated in TE due to their minimum weight combined with maximum strength, thus being able to save on material used. In addition, the fact that minimal surface scaffolds have an open cellular structure provides an ideal environment for cell migration and tissue ingrowth keeping the structure stable [11], [14]. In nature, we can see examples of minimal surface geometries in beetle shells, weevils, butterfly wingscales and crustacean skeletons [15], [16].

In order to fulfill the challenging requirements of TE, biomaterials should have specific features such biodegradability, biocompatibility, non-toxicity and good mechanical properties [10]. In this regard, alternatives to soap/synthetic surfactants will always be better choices.

Among the different classes of materials, polymers have been widely used in biomedical applications, including surgical sutures, artificial skin and organs, prosthesis, bone repair, and even in drug delivery systems [17]. Polymers are everywhere around us and they can be classified as natural or synthetic, depending on their origin source. The former can be found in nature and in the human body and it's a result of biological processes, for example, silk, wool and chitin. The synthetic ones result of a process that require chemical processes and presents some advantages over naturally sourced ones such as high quality control, the possibility to create a polymer with the desired mechanical and chemical properties and the wide range of chemical linkages that can improve the degradation [17],[18]. However, most of the synthetic polymers are non-biodegradable, have poor bioactivity. On the other hand, natural polymers have composition similar to tissues they are replacing, versatility for chemical functionalization and good biocompatibility and biodegradability.

Chitin, the most abundant biopolymer in nature after cellulose, can be extracted from crustacean shells, insects and fungi [19]. The deacetylation of chitin gives rise to chitosan (CH), which is widely explored for a variety of applications in the biomedical field due to its good biocompatibility and biodegradability as wound-healing activity, bioadhesive and antibacterial properties [19], [20]. Besides these properties, it is reported in literature that low molecular weight chitosan (LMWC) – molecular weight less than 150 kDa – can be used for preparing polymeric surfactants [21] due to surface activity of chitosan itself. In this regard, biosurfactants appeared as a potential alternative to the synthetic ones for having low toxicity and biodegradability.

The addition of inorganic compounds to an organic system provides many advantages to biophysical properties such as shape, topography, stiffness and charge of biomaterials [22]. Silica-based materials has unique properties such as mechanical robustness, chemical, mechanical and thermal stability and inertness [23], and so, the addition of a silica network onto organic components offers several advantages.

In this context, the aim of this work is the development of novel hybrid materials based/inspired on minimum surface area generated by the immersion of a specific geometry into a soap solution. This is a novel approach to create a biomaterial since usually the scaffold design used is created in advance whereas in this case, a template is used to give rise to a different structure inside. In this particular case, the solution will consist of chitosan and silica. To achieve such goal, the geometric templates will be printed using a thermoplastic 3D printer and then will be emerged in a solution of methacrylate chitosan (CH-MA) and tetraethyl orthosilicate (TEOS), which is a silica precursor that has been used in the preparation of silica-based materials. Upon crosslinking, it's expected the formation of a hybrid hydrogel with geometry similar to the figures shown below in Figure 3. These materials will be characterized regarding their chemical composition and biological behavior. Thus, in the sense of material fabrication we are faced with a bottom-up approach, while in terms of application it is considered a top-down strategy.

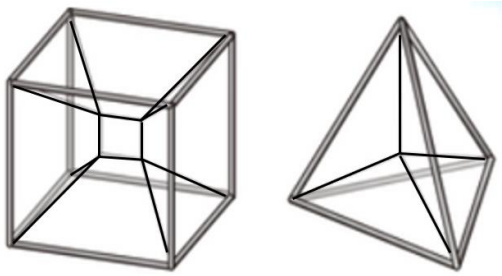

Figure 3. Shaped polymer-based structures from square and tetrahedron.

2. Introduction

2.1. Additive manufacturing

Through the need for efficient industrial production reducing the time to produce new products for the market, in mid 1980s, additive manufacturing (AM) emerged. AM is characterized by the ability to adopt designs for specific purposes, thus shortening the time between design and manufacturing while minimizing the waste for an acceptable cost [24]. AM is a layer-by-layer manufacturing technique that involves a computer-based 3D model and a 3D printer. This technique has different approaches, such as 3D printing (3DP), rapid prototyping (RP), and solid freeform fabrications (SFF). The four methods of AM widely used in TE field are stereolithography (SLA), selective laser sintering (SLS), 3D bioprinting (3DBP) and fused deposition modeling (FDM) [24], [25]. What varies among them is their method of layer manufacturing, the material and machine technology used.

FDM, also known as fused filament fabrication (FFF), is an AM technique which consists in depositing a filament of thermoplastic material. A portion of polymer filament of is fed into a heated nozzle which melt the polymer and then is extruded in the XY plane forming a 3D part [24]. After printing one layer the head moves along Z axis initiating the formation of the next layer. This technique is so useful for bone tissue engineering due to freedom in design and controllable porosity. The choice of polymer to be used depends on your application and among them are polylactic acid (PLA), polyethylene glycol (PEG), polycaprolactone (PCL) and polyvinyl alcohol (PVA). In a context of bone tissue engineering, biodegradable scaffolds prepared by FDM are being studied to be used as carriers for osteoblasts [26].

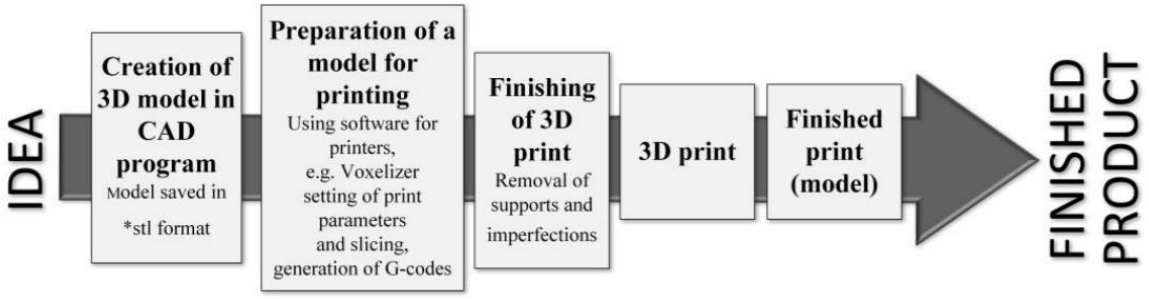

Figure 4. Step by step procedure of FDM printing. Reproduced from [27].

Figure 4 shows basic principles of 3D printing procedure by FDM technique – conceptual idea is transformed into digital data through 3D computer-aided design (CAD) model and saved in *STL* format. The next step is the slicing stage of the model into layered data just followed by the setup of some parameters at the time of printing such as feeding rate, infill, head size, table temperatures and printing path. This information will be then transformed in a G-code file by a software program (slic3r), which will be uploaded in 3D printer. Upon that, 3D printer is ready to produce a real model by melt extrusion. Finally, depending on the targeted application, some imperfections and the supports need to be removed from the 3D product [24],[27],[28].

2.2. Influence of geometry on tissue regeneration

The wide use of 3DP in TE is due to its greatest advantage – freedom in geometry of the materials manufactured, since it is known that the geometry of the scaffolds used is one of the most important parameters in TE field and controlling the geometrical design and the size of porous of scaffold is much easier to do using computational models.

The geometrical design of scaffold influences the stimulation and guidance of the regeneration process namely, cell adhesion, proliferation, differentiation as well as the responsiveness to extracellular signals [29]. In case of bone tissue engineering, it is reported in literature that parameters such as the pore size and interconnectivity of the porous structure influence the bone regeneration process [30]. Furthermore, it has been shown that the pore shape and surface curvatures also have a strong impact on it [31].

Among the various geometrical features that demonstrated to have influence on efficiency of porous scaffolds, surface curvature and pore size have received the most attention. Curvature is capable of controlling and guiding the tissue regeneration process, both nano and macroscale curvatures. Rumpler *et al.* showed that curvatures with radii larger than the cells interact with them and influence their behavior [32].

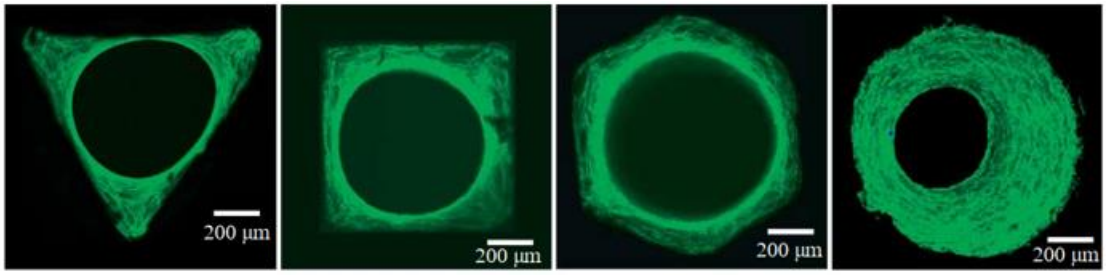

Figure 5. Staining of cell actin stress fibers to visualize the tissue formed *in vitro* and to study the effects of curvature of a triangular, square, hexagonal and round shape introduced into a hydroxyapatite plate *in vitro.* Adapted from [32].

In Figure 5, the formation of new tissue begins in the corner of structures and tissue grew uniformly on the round surface. The tissue thickness in the corners was greater in triangular structure followed by the square and then the hexagonal one, i.e, in the order of decreasing local curvature [32]. This result helps to understand that the rate of tissue generation is proportional to the curvature of the surface.

Besides the curvature, it also matters the type of curvature, that is, whether is concave or convex. It has been shown that the tissue growth process prefers concave surfaces to the convex and flat ones – Figure 6, and a potential reason for this could come from the high contractility of the cells themselves [33].

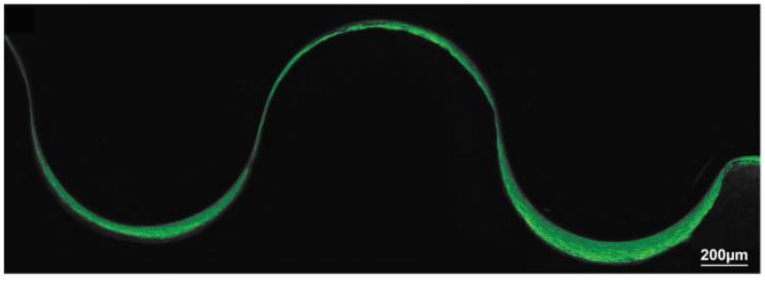

Figure 6. Confocal images of tissue stained for actin (green) on a wave-like substrate with the scaffold below and medium above. Reproduced from [33].

Pore shape in scaffolds could range between simple geometrical shapes such as cubit unit cells to more complex ones such as diamond-type unit cell, and even advanced shapes such as minimal surfaces [14], [34]. Geometrical features with a higher curvature leads to higher levels of stress concentration, and, thus, higher levels of tissue regeneration stimulus [35]. The dependence of tissue growth on the curvature could be explained by the presence of contractile tensile stresses produced by cells near the tissue surface [33] and this make clear the importance of surface tension in tissue regeneration.

One of the biomimetic approaches in the design of porous scaffolds for bone tissue engineering has been based in the structure of bone and trying to replicate that in the scaffolds fabricated. It is reported that the average mean curvature of trabecular bone is shown to be close to zero [36] and this remark is linked to the definition of minimal surface – geometry that locally minimizes their surface energy, which is equivalent to having a mean curvature of zero [11]. So, it is normal to consider minimal surfaces for the design of bone tissue engineering scaffolds having in mind that they are lightweight construction materials [14] .

Actually, a specific class of minimal surfaces, triply minimal surfaces – Figure 7, has been widely studied and proposed for the design of porous scaffolds for bone regeneration applications due to their higher surface area volume ratio compared to the conventional lattice scaffolds [14],[37].

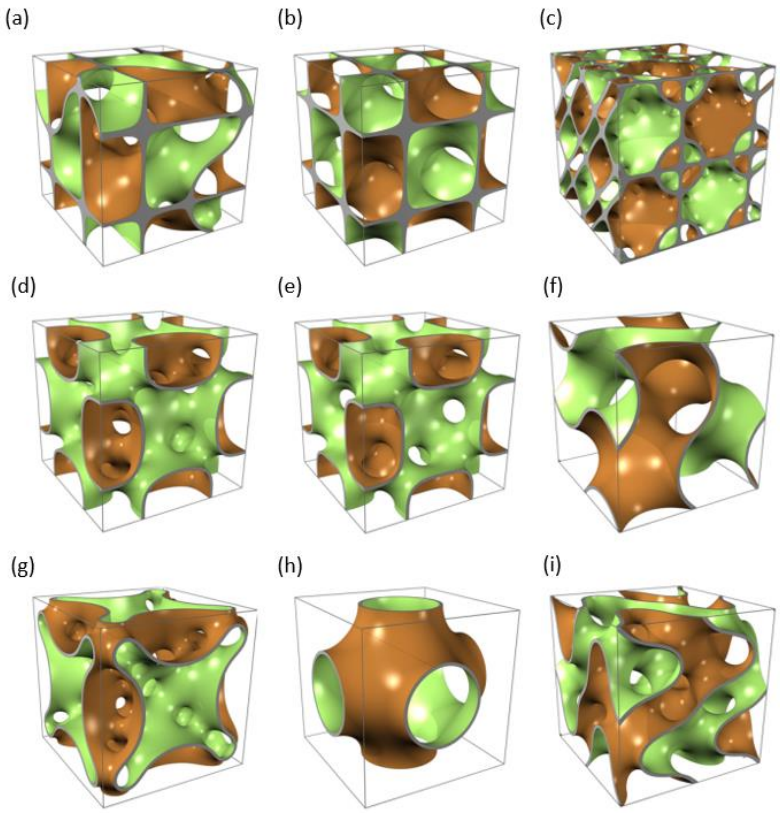

Figure 7. Examples of triply periodic minimal surfaces. Shown are translational unit cells of (a) C(Y), (b) Diamond, (c) C(D), (d) Batwing, (e) F-RD, (f) Gyroid, (g) Manta 35, (h) Primitive, and (i) Fischer Koch S. Reproduced from [14].

2.3. Minimal surfaces

By definition, a surface is minimal if its mean curvature is zero which is equivalent to say that it is a critical for area. In non-mathematically terms, minimal surfaces are like soap films – these films form a minimal surface area between given boundaries. Besides a mean curvature of zero resembles the mean curvature of trabecular bone which is also known to be close to zero [36],[38]. Minimal surfaces are frequently found in nature and in tissues of some species, playing an essential role in guiding chemical, biochemical and cellular processes [32],[39]. As examples of minimal surfaces geometries in *in-vivo* biological tissue, there are beetle shells, butterfly wingscales and crustacean skeletons [14],[15],[16]. Minimal surfaces are also present in atomic organization of molecules and in the lipidic bilayer of cellular membranes [40],[41].

The natural organization of minimal surface structures follows the physical principle which governs the nature in general and the forms and motions of objects, the principle of free energy minimization. In nature, systems try to arrange themselves to reduce their potential energy to the lowest possible potential energy that a surface can have if its energy is proportional to the surface area, in order to consume less energy as possible, increasing their stability [42]. This minimization of surface energy leads to typical curved structures with respect to the fixed frontiers – Figure 8 [43].

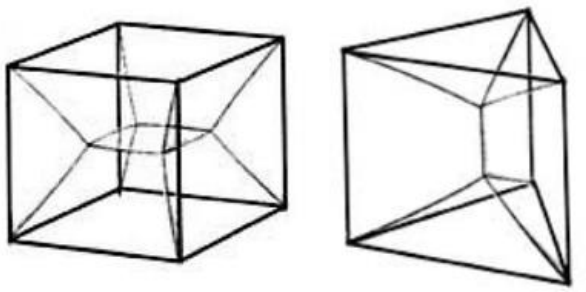

Figure 8. Minimal surfaces defined by soap films on cubic and triangular prismatic wire frames.

The minimal surface of a cube connects all the edges and have the walls sloped inside, meeting angles of 120 degrees around the small square that is formed at the center of structure. Considering the cube represented in Figure 8, it seems that each six faces of the cube make the soap film, however, in fact, 13 soap films are made on the frame; 12 faces of film are pulled internally from 12 sides towards the cubic center and one more, the thirteenth square of soap film is made at the center [44], [45]. With another prisms and complicated forms leads to the same result – at the point where each soap film intersects, they intersect in three faces. It never becomes four or more faces, and the intersection angle is 120 degrees [12],[13].

The characterization of an equilibrium surface lies in the curvature of the surface or film. If the surface is a circle with radius R, curvature *K* is defined by the inverse of radius, as represented in Eq. 1 [12], [13]. Large circles have small curvature, and vice versa. This goes along with the concept of a straight line having no curvature and being equivalent to a circle with infinite radius [13].

$$\kappa = \frac{1}{R} \qquad Eq.1$$

When we have a surface with three dimensions, we will have several curvatures whose values depend on the cross section considered. Two principal curvatures, κ_1 and κ_2, which will be the maximum and minimum curvatures existing within a normal section through the point of interest on the surface – Figure 9 (a). For a saddle point, a point in surface that has zero slope, is easy to see the sections to use – the *xz* and *yz* planes represented in Figure 9 (b) [13].

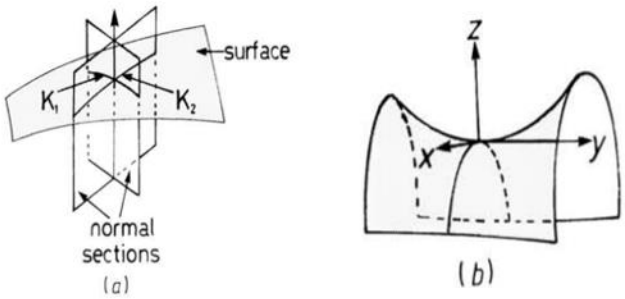

Figure 9. (a) Illustration of principal curvatures for a surface. (b) Principal curvatures for a saddle point. Reproduced from [13].

The principal curvatures are in orthogonal planes and only the two principal curvatures have this orthogonality. Normally, the direction of one principal curvature is clear, and then it's easy to find the another one by the orthogonality principle [13]. Now, one can define Gaussian curvature κ as

$$\kappa = \kappa_1 \kappa_2 \qquad Eq.2$$

and a mean curvature H as

$$H = \frac{\kappa_1 + \kappa_2}{2} \qquad Eq.3$$

And as mentioned before, a minimal surface being characterized by zero mean curvature means that

$$H = 0 \quad or \quad \kappa_1 = -\kappa_2 \qquad Eq.4$$

The physical explanation of this lies in the Laplace-Young equation represented in Eq. 5 which relates the pressure variation among the surface, where R_1 and R_2 are the maximum and minimum radii of curvature

$$\Delta p = \alpha \left(\frac{1}{R_1} + \frac{1}{R_2}\right) \qquad Eq.5$$

For the pressure difference to be zero, the pressure on the outside must equal the pressure on the inside, and for this to happen there, must be a positive and a negative radius of curvature, $R > 0$ and $R < 0$, respectively, and so we are faced with saddle point of the surface [46].

Minimal surfaces satisfy all the equations shown above, reaching the equilibrium and stability by minimizing their surface energy. As can be seen through Figure 8, the films formed by soap, in both geometries, have zero mean curvature – their principal curvature planes (the films that are created inside the cube and triangular prism templates) are equal and opposite at every point, canceling each other giving rise to a minimal surface.

2.4. Hybrid materials

Organic/inorganic hybrids display characteristics of organic polymers and ceramics and they achieve properties that a single phase material cannot give [47], [48]. In general, the organic polymer components of such materials have good elasticity, low density, formability, while the inorganic components are hard, stiff, and thermally stable. Together, these materials can produce hybrid materials which are chemically stable, with better mechanical properties, cytocompatibility, and with controllable bioactivity [49], [50].

These composites are easily produced by sol-gel chemistry, which is a very versatile method allowing incorporation of inorganic component like metal alkoxide like Si, Ti, Zr or even bioactive materials, at low processing temperatures [51]. The inorganic phase is obtained from metal alkoxides via hydrolysis and condensation reactions in the sol-gel process. In the case that both organic and inorganic components are physically bonded, the obtained material is classified as the class I hybrid. If material arise from sol-gel method, a covalent coupling is obtained between the organic and inorganic networks, and the material is classified as the class II hybrid [50]. The major advantages of sol-gel are its mild condition, simplicity and nature of starting material variation. The properties and structure of materials prepared by this method could be controlled by various parameters, such as pH of reaction, temperature, reaction time, precursor used and catalyst [52]. Sol-gel method is particularly useful because they allow to produce a several materials in different forms (coatings, fibers, foams, etc) without using expensive processing technologies.

One very attractive silica precursor is tetraethylorthosilicate (TEOS), due to its compatibility with a variety of biopolymers, including chitosan [51]. The main reason to choose TEOS is that the formation of robust networks with moderate reactivity and a high degree of control related with simple variations in the synthesis conditions mentioned above. After hydrolysis reactions, the composition of TEOS includes silanol groups (Si-OH) that are easy to bind with the hydroxyls, and with amines present in chitosan, in the presence of ethanol, acid, and water through sol-gel method giving rise to chitosan/TEOS composites (Figure 10) with greater ceramic nature and improved characteristics such as thermal, mechanical, optical and adsorbency [53].

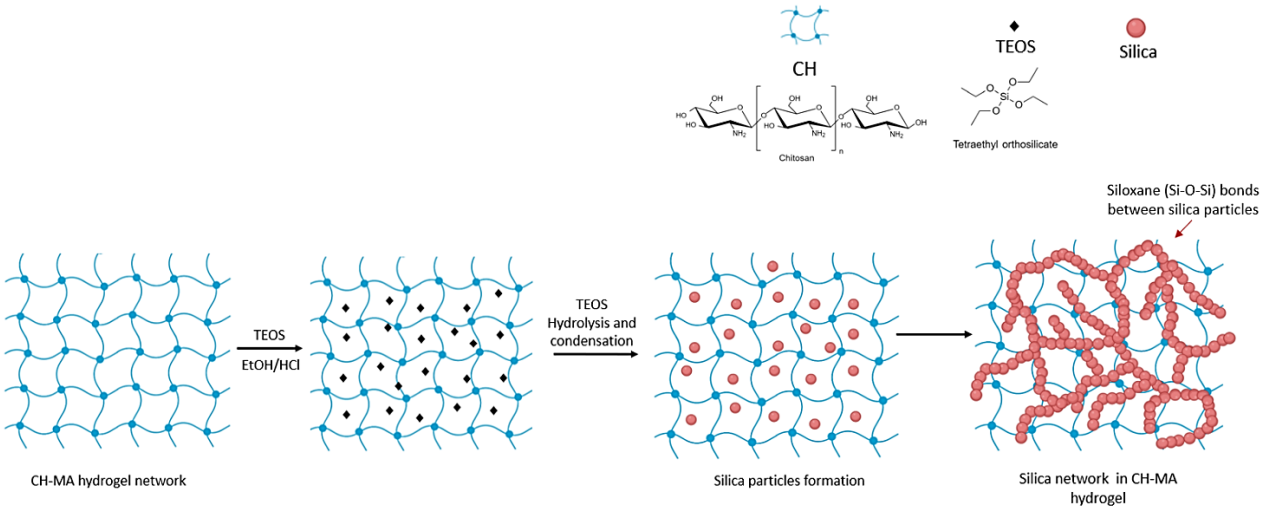

Figure 10. Schematic representation for preparation of chitosan siloxane (CH-Si) hybrids.

Chitosan is a multifunctional natural polymer, which is obtained when the degree of chitin deacetylation is at least 60%, is a linear polysaccharide composed of glucosamine and N-acetylglucosamine units linked by β (1-4) glycosidic bonds (Figure 11) [19]. Physicochemical characteristics of CH, including its biodegradability, bioactivity, viscosity, solubility and crystallinity, are inversely influenced by the molecular mass and degree of deacetylation.

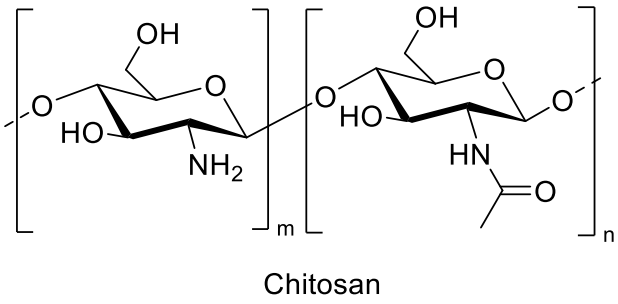

Figure 11. Chemical structure of chitosan.

Despite the advantages of CH reported above, their high molecular weight difficult water solubility at a neutral pH and their viscosity limits its application in a numerous field such as food, health, and agriculture. However, it is reported in the literature that low molecular weight chitosan (LMWC) i.e., molecular wight less than 150 kDa, has been use in the preparation of polymeric surfactants [54]. LMWC can be used as one of the basic materials for synthetizing different polymeric surfactants. These surfactants display good properties like biodegradability, biocompatibility, and bioactivity.

Surfactants (SURFace ACTive AgeNTS) are in widespread use in a range of applications, functioning as detergents, wetting agents, emulsifiers, and foaming agents. Surfactants can be

classified as synthetic or biological, depending on their origin. They are amphiphilic compounds that contain both hydrophilic – water soluble head - and hydrophobic groups – tail [55]. Due to this structure, these substances have the ability to diffuse in water and to place themselves between air/ water or oil interface, thus reducing surface tension and stabilizing systems. The critical micelle concentration (CMC) is an important characteristic for surfactants. CMC is the concentration of a surfactant in a bulk phase, above which surfactant monomer molecules associate to form micelles, bilayers and vesicles – Figure 12.

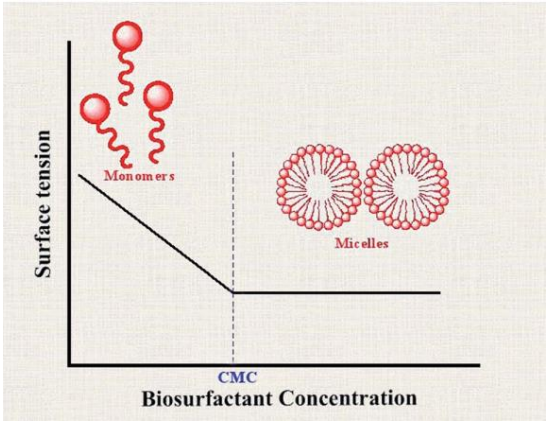

Figure 12. Relation between surface tension and biosurfactant concentration and formation of micelles. Adapted from [55].

This is the property that enable surfactants to minimize the surface tension and enhance the solubility of nonpolar compounds [55]. However, beyond a certain concentration, increasing a concentration of surfactant do not lead to further reduction in surface tension. The CMC is usually used to measure surfactant efficiency. More efficient biosurfactants have lower CMC, i.e. less biosurfactant is needed to decrease the surface tension [56]. Most of the surfactants used nowadays are synthetic and these are used in large quantities in industry every day. However, these materials are very toxic and present low biodegradability causing a great negative impact on the environment. Thus, biosurfactants appeared as a potential alternative to the synthetic ones. Natural surfactants or biosurfactants are amphiphilic biological compounds produced by a various number of microorganisms. They present low toxicity, functionality under extreme conditions, lower CMC that those synthetic surfactants, and they are biodegradable [55]. The major challenges for the use of biosurfactants lies in the fact of low production yields, expensive purification processing and lack of appropriate understanding of the bioreactor systems for their production [55], [57].

CH can be modified using different functional groups and/or inorganic compounds to obtain derivatives with improve properties [58]. These derivatives compounds are created by reactions of the hydroxyl and amine groups with appropriate reagents. The presence of primary amine groups as well as hydroxyl groups allows its derivatization and the introduction of functional groups via covalent or ionic bonding with silica precursors [59].

The combination of inorganic and organic networks, such chitosan-silica based materials, by sol-gel method facilitates the design of new engineering materials with diverse improved properties for a wide range of applications in tissue engineering – Figure 13. The gel derived materials are excellent for studying and controlling biochemical interactions within constrained matrices with enhanced bioactivity because of the chemistry of their surface [49], [50]. In biomedical applications, the coating of medical devices is an important issue. They should have appropriate mechanical and chemical properties to promote a healing response without causing adverse immune reactions [50]. Biologically stable hybrids can be used in bioreactors systems and as scaffolds in TE. Biodegradable scaffolds are widely used in TE while the biostable ones that can hold globular aggregates of cells are suitable for bioreactors [49].

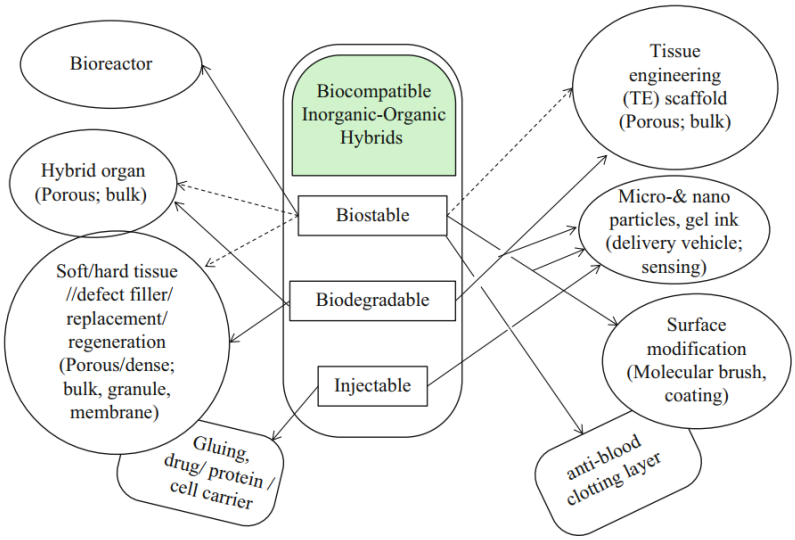

Figure 13. Major biomedical applications of inorganic-organic hybrids depending on their specific properties: biostability, biodegradability, and injectability (fluidity). Reproduced from [49].

3. Materials and methods

Chitosan (CH) (Av. Mw 96365 Da, 97.24% deacetylated), Tetraethyl orthosilicate (TEOS) (98% pure), Methacrylic anhydride (MA), Lithium phenyl-2,4,6-trimethylbenzoylphosphinate (LAP), cellulose membrane dialysis tubing (MWCO 3.5 kD) and Fluorescein isothiocyanate (FITC) were purchased from Sigma-Aldrich. Hydrochloric acid (PA ≥37%) and Nile Red was obtained from Laborspirit, Acetic acid glacial (AA) from JMGS and Ethyl Acetate (99.94%) from LABSOLVE. L929 mouse fibroblasts cells were purchased from ATCC® (American Type Culture Collection) and used from passage 17 to 23, Dulbecco's Modified Eagle's Medium Low Glucose (DMEM-LG) and Trypsin-EDTA were purchased from Sigma-Aldrich (USA). Fetal Bovine Serum (FBS), 1% (v/v) antibiotic/antimycotic, DPBS (PBS without calcium and magnesium) and Calcein-AM/Propidium iodide (PI) (Live/Dead Kit) were obtained from ThermoFisher Scientific. Formazan-based colorimetric assay (CellTiter 96® Aqueous One Solution Cell Proliferation Assay) was supplied by Promega.

3.1. Additive manufacturing of sacrificial templates

All templates were designed in SOLIDWORKS® (2020/2021 Academic version provided by University of Aveiro) software and then exported to STL format files. These files were processed by Slic3r Prusa Edition to generate G-code instruction for the 3D printer. Different geometries were printed using PLA via a 3D printer (PRUSA ultra). The extrusion was carried through 0.4mm nozzle, at an average speed of 40 mm/s (which may vary in some layers) and under 220ºC.

3.2. Modification of chitosan with methacrylic anhydride (CHT-MA)

The modification of CH was performed following a procedure described in the literature [60] and is represented schematically in Figure 14. Photo-crosslinking CH was prepared dissolving 2% (w/v) of CH to a 2% (w/v) AA solution (pH 5.5) and this one was allowed to react for 24h at room temperature (RT). Following, $4.4x10^{-2}$ mol of methacrylic anhydride (corresponding to 2 molar equivalents per CH mol) was added to the previous solution and react for 24h at RT. The prepared polymer solution was dialyzed with a molecular weight cutoff of 3.5 kDa dialysis tubing against distilled water for 1 week. Water was replaced every day, once a day. The purified CH solutions were stored at -80ºC and then lyophilized over a week and stored at 4ºC, protected from light until further use. The substitution degree (SD) was determined by the ratio of the integral area of the peaks corresponding to the two hydrogens adjacent to C=C bond (located at 5.68 and 5.30 ppm, respectively) and the integral area of the peaks corresponding to the Glucosamine rings (3.46 – 2.74 ppm) [60], achieving a SD of 14.3 %.

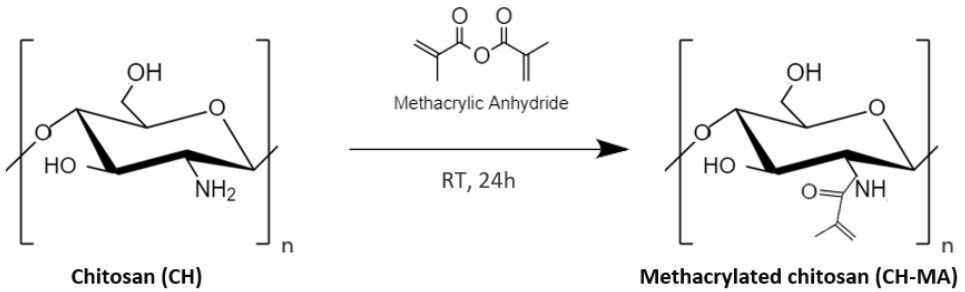

Figure 14. Schematic representation of the chemical modification of chitosan (CH) with methacrylic anhydride (MA).

3.3. Fabrication of CH-MA–Silica Hybrid Hydrogels by Photo crosslinking

The method to prepare hybrid scaffolds is represented in Figure 15. The 3% chitosan solution was prepared by dissolving the lyophilized CH-MA in purified water at a pH=5 with LAP (0.5% w/v) as a photoinitiator. Hybrids were prepared based in sol-gel reaction using TEOS, as silica precursor, and HCl 10% as catalyzer. Solution consisted in TEOS/water/ethanol/HCl mixture with molar ratio 3/15/1/0.0185. This solution was stirred for 24h and then 1 mL of it was removed and added to the 15mL of 3% chitosan solution previously prepared.

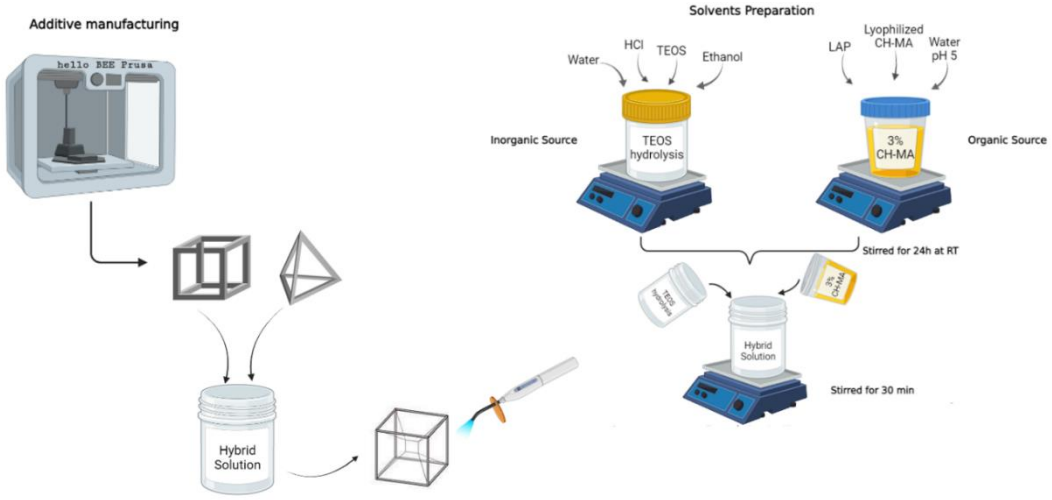

Figure 15. Materials and methods for preparation of hybrid scaffolds.

Following, the templates manufactured by 3D printing, were dipped into this hybrid solution and removed until the desired scaffold shape was achieved through the minimum surface tension of the geometry used. Then, to solidify the suspended liquid films, photo- crosslinking was induced with VALO Cordless® (multiwavelength light-emitting diode -LED) (t=120s) and gel-like solutions were obtained. These gels were allowed to dry at RT for, approximately, 48 hours. To remove the polymer templates (PLA), the structures were immersed in ethyl acetate for ≅ 20 hours, remaining only the minimalistic hybrid 3D structure.

3.4. Characterization of hybrid material

3.4.1. Scanning electronic microscopy (SEM) and Energy Disperse X-ray spectroscopy (EDS)

A Scanning Electron Microscope (Hitachi - TM4000Plus) was used to examine the surface and hybrid composition of samples coupled with an EDS (Bruker, Quantax 400 detector).

All samples underwent a deposition of a thin carbon film with the objective of giving them electrical conductivity. To this end, the fiber samples were placed on carbon tape in the flat and polished aluminum sample holders.

3.4.2. Fourier transformed infrared spectroscopy (FTIR)

This method was carried out in the Chemistry department of the University of Aveiro being that the spectra were obtained in a spectrometer of Bruker brand, model Tensor 27, with a resolution of 4 cm^{-1} and 256 scans. These were acquired at 4000 to 350 cm^{-1} range.

3.4.3. Proton nuclear magnetic resonance microscopy (NMR)

^{1}H NMR analysis were recorded at 70ºC on a Bruker Advance III 400 MHz spectrometer. The sample characterized was previously dissolved in 800 µl of D_2O and then transferred to 300 MHz NMR glass tubes (Sigma-Aldrich). The spectra acquisition parameters consisted of 256 scans and 18s relaxation delay. A software called MestReNova was used for processing the data.

3.4.4. Thermogravimetric analysis

Thermogravimetry analysis was performed in this work using a simultaneous thermal analyzer (HITACHI STA 300 – Thermal Analysis System) of temperature ranging from 30º-800ºC at 10ºC min^{-1} heating rate of 20 ml min^{-1} nitrogen flow rate. The data was used to study the hybrid composite and the organic one.

3.4.5. Fluorescent microscopic characterization of 3D structures

Fluorescent CH was prepared as previously reported [61]. Briefly, FITC was dissolved in ethanol (EtOH) (0.05% *w/v*) and this solution was added to a solution of 2% *(w/v)* CH in distilled water (DW). Then, the solutions were stirred at RT for 24h in the absence of light. The next step is to remove the unreacted FITC via centrifugal separations at 4000 rpm for 10 minutes using EtOH. The final product was obtained as a powder by using a vacuum dryer at RT for 24 h. In order to stain the silica, Nile Red (0.1% w/v) was added to the TEOS/water/ethanol/HCl solution in a proportion of 1:5 and then, this mixture was added to chitosan solution and stirred for 30 min. To observe the different samples, a Widefield microscope (Zeiss, Axio imager 2) was used.

3.4.6. *In vitro* cell culture

L929 mouse fibroblasts cells were cultured with DMEM-LG supplemented with 10% (v/v) FBS and 1% (v/v) of antibiotic/antimycotic. Cells were expanded in 75 cm^2 T-Flasks at 37ºC in a humidified air atmosphere of 5% CO_2. The medium was changed twice a week. Upon 90% of confluence, cells were detached via 0.05% w/v trypsin treatment for 5 min at 37ºC. Cell suspensions were then recovered by centrifugated for 5 min at 300g and then seeded for the different assays.

3.4.7. Live/dead assay

To evaluate cell viability, hybrid and CH scaffolds were incubated in Calcein-AM/PI for 20 min. This assay was performed for 1 and 7 days. Cells were seeded in contact with hybrid and CH-MA samples at a density of 2 x 10^4 cells (for day 1 timepoint) and 2.5 x 10^3 (for 7 days timepoint) on 8-well IBIDI plates. Widefield (Zeiss, Axio imager 2) microscope system was used to visualize the stained cells. Acquired data was processed in Zeiss ZEN v3.1 blue edition software.

3.4.8. Bioactivity assay

Simulated Body Fluid (SBF) pH 7.4 was prepared following a procedure described in the literature [62] and stored at 4ºC until further use. Hybrids and CH structures were immersed in approximately 15 mL of SBF and incubated at 37ºC for 14 and 21 days. The SBF solution was renewed after 14 days. After each timepoint, the samples were washed using DW to remove soluble ions. The formation of apatite layers on the surface scaffolds was examined by SEM. Element composition of the apatite was examined using an energy dispersive x-ray spectrometer (EDS) equipped within the SEM equipment.

3.4.9. MTS viability assay

Scaffolds cytotoxicity profile was evaluated using a formazan-based colorimetric assay at days 1 and 7 of culture. Mitochondrial dehydrogenase enzymes of encapsulated viable cells are able to convert 3-(4,5-dimethylthiazol-2-yl)-5-(3-carboxymethoxyphenyl)-2-(4-sulphofenyl)- 2H-tetrazolium (MTS) into a cell culture soluble brown formazan product. Briefly, four samples of each material (hybrid and CH-MA) were placed in 96-well plate in contact with L929 cells for 1 and 7 days seeded at densities 2 x 10_4 cells per well and 2.5 x 10_3 cells per well, respectively. Then, 20 µl of MTS solution and 100 µl of media were added to each well, and subsequently incubated for 4h at 37ºC and 5% of CO_2. After the incubation time, 80 µl of supernatant of each condition was transferred to another 96-well plate and the absorbance was measured at 490 nm using a microplate multimode reader (Gen 5 2.01, Synergy HTX, Bio-TEK).

3.5. Statistical analysis

All data were exhibited as the average $\pm$ standard deviation (SD) and the statistical comparison was examined by the one-way analysis of variance (ANOVA). A $p < 0.05$, $p < 0.01$ and $p < 0.001$ were considered significant.

4. Results and Discussion

4.1. Synthesis and Characterization of Modified Chitosan

CH was modified with methacrylic groups to promote the formation of covalent bonds within the chemical structure. The introduction of methacrylic groups enables the photo-crosslinking in the presence of a photointiator, in this specific case the LAP, to enable the formation of covalent bonds. The ^{1}H NMR spectrums of CH and CH-MA are represented in Figure 16.

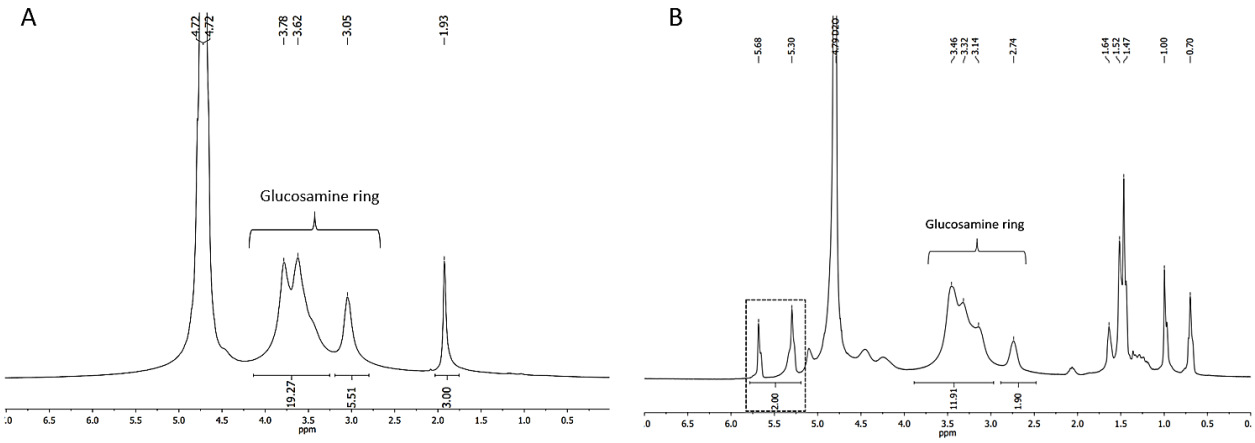

Figure 16. ^{1}H-NMR spectrum of (A) CH and (B) CH-MA in D_2O.

The Figure 16 shows the NMR spectra of CH before and after methacrylation. The peaks at 3.05-3.78 (Figure 16-A) and 2.74-3.46 (Figure 16-B) ppm are the protons in the ring of the glucosamine. The single peak at 1.93 ppm in (A) corresponds to the acetyl group of CH. The two peaks at 5.30 and 5.68 ppm in (B) are due to the methylene and methacrylamide and indicate that CH was methacrylated. The peaks from 1.47 to 1.64 ppm were assigned to protons on the amino, hydroxyl and methyl groups in the acetyl and methacrylamide moieties [63], [64].

4.2. Hybrid scaffolds/ Surface tension-based materials

The hybrid scaffolds were prepared by immersing the PLA templates into the hybrid solution and then photopolymerize -under curing light while 120 seconds. The templates were dipped into the solution two times each, to improve the thickness of hydrogel. Figure 17 shows the produced tension-based hybrid scaffolds. In Figure 17-A, the scaffolds are freshly prepared as can be seen by their transparent appearance, meaning that they are still in hydrogel form. When left for two days at RT, the hydrogel eventually dries giving rise to the appearance shown in Figure 17-B.

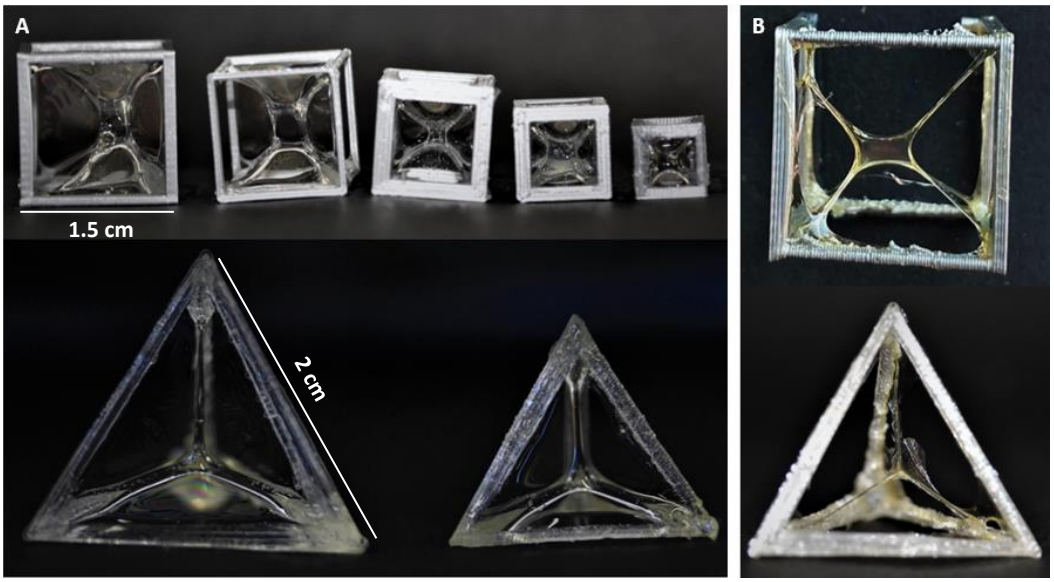

Figure 17. Tension-based scaffolds after being photocrosslinked (A) in hydrogel form and (B) dried forms.

To sacrifice the PLA templates, that is, to remove them, the structures were immersed in ethyl acetate for 1 day. Then the PLA thermoplastic starts to detach from the biomaterial, thus obtaining the scaffold as represented in the figure 18 (B). The primary analysis reveals that the obtained structures are contractile but also fragile. At macroscopic view, both organic and hybrid dried scaffolds do not seem to have any differences, but by handling can be concluded that the stiffness of hybrid scaffolds is greater than the pure CH scaffold.

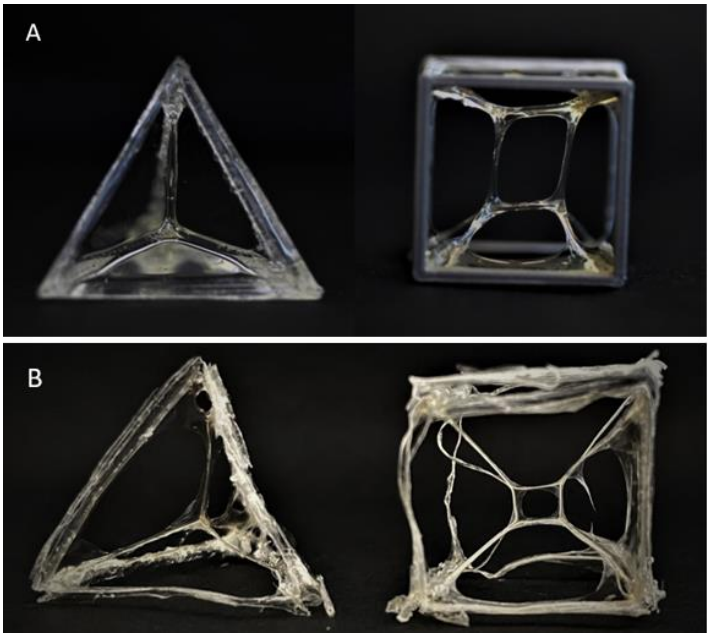

Figure 18. Hybrid scaffolds (A) attached to the PLA template and (B) after template sacrifice.

With the aim of confirming whether the manufactured scaffolds can really be considered minimalistic materials, one of the higher size sacrificed scaffolds was weighed – Figure 18-A and then, the same amount of material (3% CH-MA solution, in this case) was freeze-dried. The CH-MA sponge obtained is represented in the Figure 18-B. Although it was possible to obtain a non-compact sponge with this amount of freeze-dried material, it is not sufficient to recreate another minimal surface scaffold through it (i.e., create another 3% solution through this sponge and give rise to another minimal surface structure). However, it is reported that CH sponges obtained by freeze-drying derived from 1-4% CH solutions has good biomechanical properties and can be employed as a carrier of growth factors due to its structural, mechanical and releasing properties [65]. In concluding form, the fabricated scaffolds can be classified as minimalistic materials.

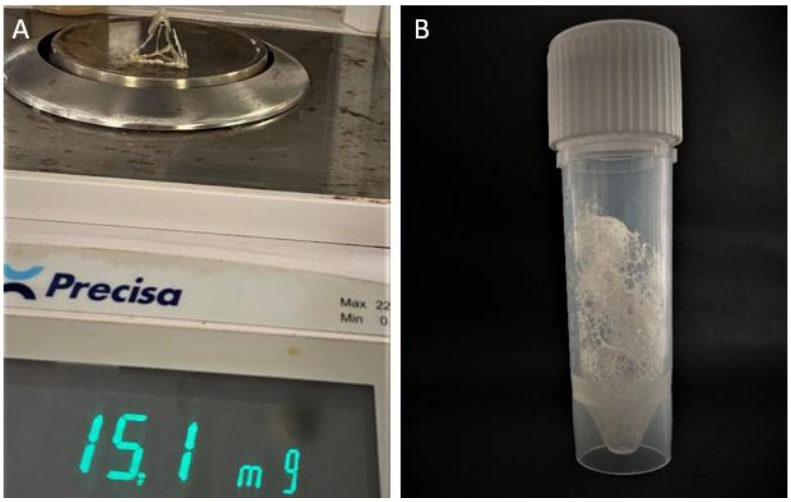

Figure 19. (A) Weight of the minimal surface scaffold; (B) Sponge obtained by freeze-drying using the same amount of material weighed.

Given that a minimal surface scaffold was successfully obtained, the next step was to attempt to go from one unit structure to a scale up – Figure 20. As can be seen in the images, the minimum energy geometry is alternately formed along the template – Figure 20-A.

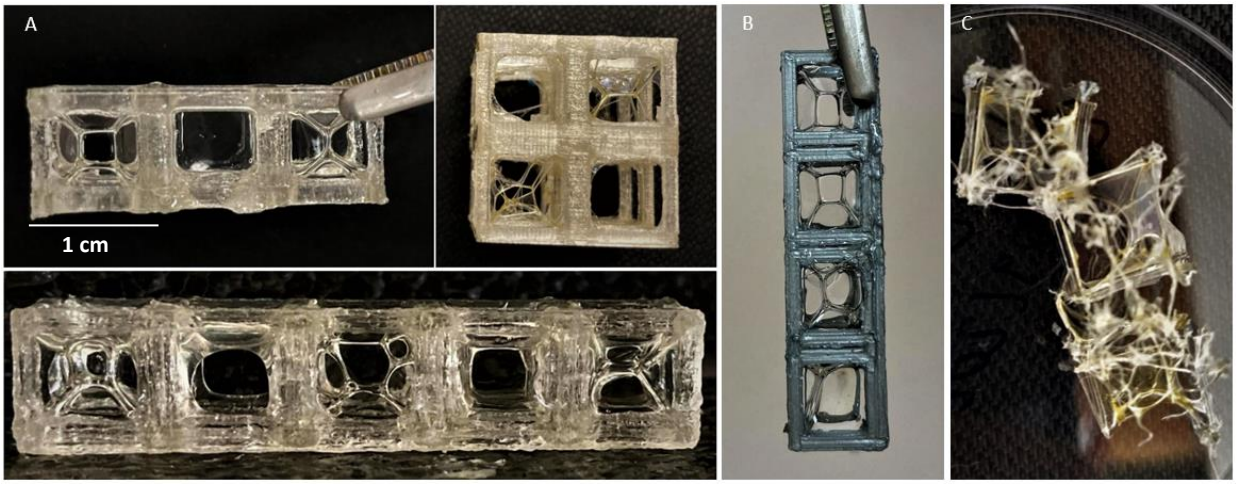

Figure 20. (A) 3D scaffold with cubes in linear connection; (B) 3D scaffold with an extra interface between cubes; (C) Scaffold with 3 cubes in line after template sacrifice.

The physical principle lies on the fact that when 2 cubes are joined together, the surface tension-based film that is created can only choose one of these cubes because between the 2 cubes there is only one interface available. And for the minimal energy structure to be formed, it requires all 6 faces of cube to be free/disponible. On the structure with the 3 cubes in line (Figure 20 A), from the moment that minimal surface geometry is formed inside the cube that is at the end, the cube in the middle is left with only 5 free faces because the interface between the cubes is common to both. Since the interface is already occupied by the minimal surface film of the end cube, it cannot form the minimum energy geometry in the middle cube. Since in the middle cube the interface closest to the cube at the other end is available, the formation of the minimum energy geometry at this cube is possible. Now, the middle cube remains with only 4 flat faces free. In conclusion, when a minimal surface structure is formed inside a cube, the cube just next to it does not have enough surface energy to give rise to another minimal surface structure. There is no direct evidence in the literature indicating that minimal surfaces cannot share the same interface, but it is possible to point out many features of the material used that may contribute for such end, like its chemistry, hydrophilicity profile and electrostatic interactions [66], [67]. In this particular case, where a positively charged polymer was used, more emphasis will be placed on electrostatic interactions.

To tackle such bottleneck , an additional interface between the cubes was created as shown in Figure 20-B. As we can see, this approach was successfully employed giving rise to the fact of having the minimum energy structure in every cube. However, another limitation was observed upon the releasing of the structures from the PLA template which was the non-interconnection between the units that formed the assembled scaffold – the cubes were obtained individually – Figure 20-C. Thus, a new design of 3D scaffolds (interconnected) that enables the formation of minimal surface geometry at every structure is required.

4.3. Morphological and chemical characterization through SEM and EDS

The images acquired by SEM allowed the observation of the surface microstructures of CH-MA (Figure 21) and hybrids (Figure 22, left). To verify the presence of the inorganic compound in the hybrid formulations (Table 1), EDS analysis was carried out as can be seen in Figure 22 (right).

Table 1. Sample characteristics observed in SEM/EDS.

Hybrid	Organic:Inorganic volume ratio (ml)	Solution temperature (ºC)	Observations
A	15:1	Room temperature	Surface tension has formed in the structure
B	15:1.6	37	The solution condensed – surface tension couldn't be formed in the best way
C	15:1.6	37	Surface tension has formed in the structure

By the Figures 21 and 22 (left) it is noticeable that the scaffolds are amorphous, with no presence of pores in any of the structures. The hybrid A was obtained by adding 1 mL of TEOS solution to the 3% CH-MA solution at room temperature and the samples B and C were prepared through the addition of 1.6 mL TEOS solution to the 3% CH-MA solution at 37ºC. The difference between the 2 lasts formulations is that the sample B gelled, due to the silica condensation and the C did not gelled because this one stayed less time under agitation comparing to hybrid B.

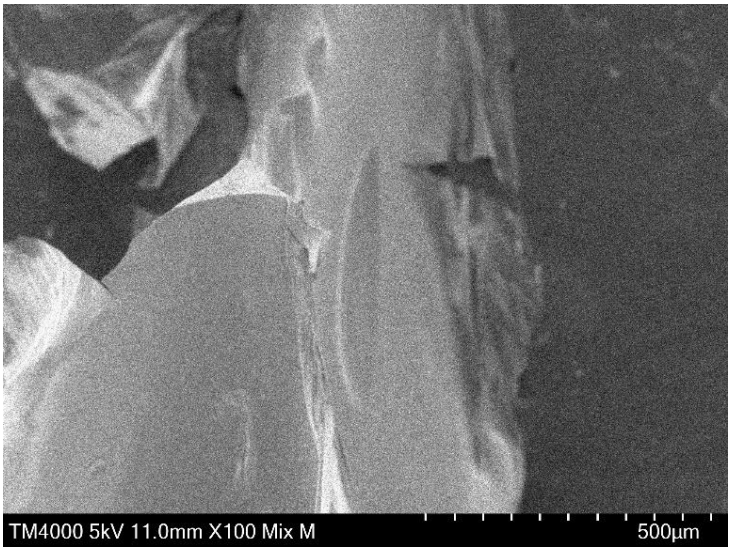

Figure 21. Morphological image of CH-MA scaffold by SEM.

Looking at the SEM-EDS spectra and images (Figure 22, right), it can be concluded that sample B contains the highest percentage of silica in its composition, followed by samples A and C, respectively. The result of the amount of silica in sample B is in line with expectations, since it

contains a greater amount of silica precursor in its composition compared to sample A (see table 1). However, looking at the SEM images and the silica distribution map, sample A has more uniformly distributed silica than sample B. This result lies in the fact that with the increase of gelation temperature, the gelation time decreases and this results in some morphological changes in the resulting material such as a formation of spherical aggregated particles and a decrease in surface area [68]. Due to greater solubility at higher temperatures, the size of silica particles within the sol increase as temperature increase [69], [70]. Thereby, and through the Table 1, it is known that sample B was heated to a temperature of 37°C which facilitated the condensation of silica and consequently the formation of aggregated silica particles in the solution and, consequently, in the hybrid scaffold. In addition, the solution condensed to such an extent that the desired minimal surface structure could not be formed in the templates.

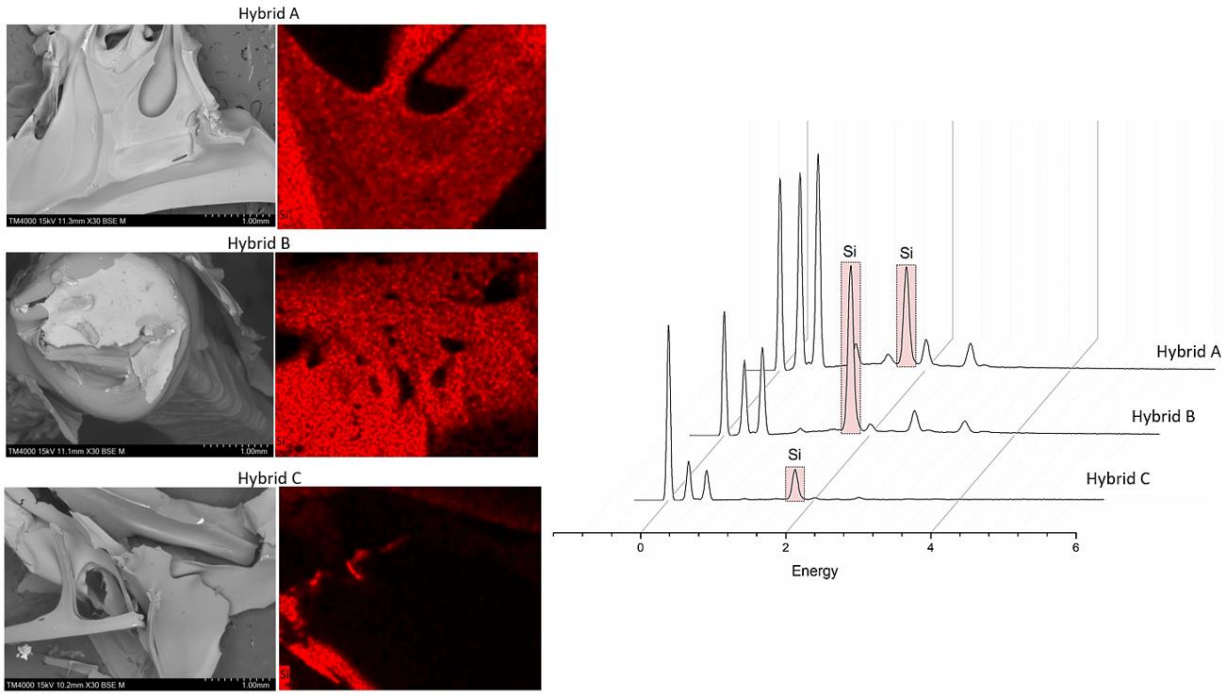

Figure 22. *SEM images (left) and elemental composition (right) of the three formulations of hybrid solutions.*

In the hybrid C, which contain the same amount of TEOS as sample B and was heated at the same temperature but for less time, so the solution did not gelled, and therefore it was possible to form the structure based on surface tension. Analyzing the elemental composition and the SEM images of this sample, the conclusion reached is similar to that of sample B: the fact that the silica particles have condensed more easily due to the temperature forming particles aggregates, therefore silica is not uniformly distributed throughout the structure, hence the peak of silica detected was lower than in sample A despite having more silica in its composition. These results are in agreement with some studies reported in the literature [68], [70], where the presence of high temperatures had the same effect on the resulting structures, that is, the formation of aggregates thus impairing the silica distribution.

Morphological structure and elemental composition given by SEM-EDS allows to conclude that the best sample to continue working is the sample A because although is not the sample with the

highest amount of inorganic in its composition, it is the only one that shows homogeneity in the distribution of silica along the scaffold and allows to form minimal energy structures.

4.4. Fluorescence microscopy characterization of the produced structures

The hybrid structures were evaluated using fluorescence microscopy, where TEOS was stained with Nile Red and CH-MA presented autofluorescence in green channel. Initially CH-MA was stained with FITC in order to observed in green channel, but the intensity of signal obtained was too high and, as it is reported in the literature that CH presents autofluorescence in green [71], CH was not stained with FITC again.

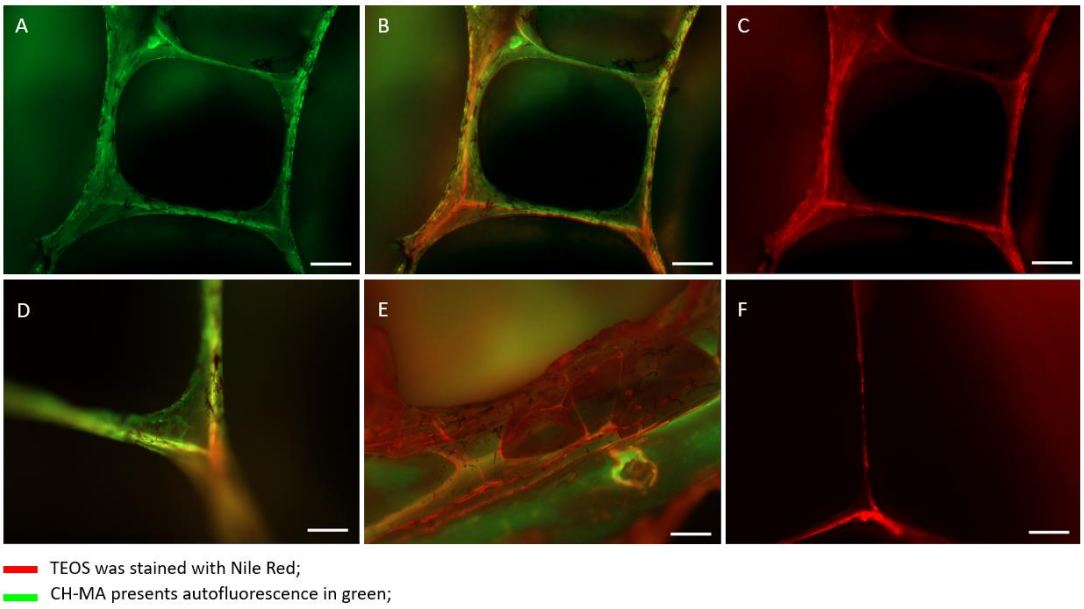

Figure 23. Fluorescence images of hybrid scaffold. TEOS was stained with Nile Red, and CH-MA presents autofluorescence in green. The scale bar corresponds to 200 µm. (A) and (D) CH-MA fluorescence in green channel; (B) and (E) both channels (green and red) opened; and in (C) and (F) the Nile Red channel is opened. All images are at 5x, except for (E) which is at 10x.

In the Figures 23 (A and D), is represented the autofluorescence of CH-MA in green channel. As can be seen through Figures 23 (B and E), where are visible the two channels, silica (represented in red) is well distributed along the structure. This confirms that the silica network is present within the CH matrix and that hybridization of CH/silica was successful. For a better perception of silica distribution along the structure, the images (C) and (F) show what can be observed in the Nile Red channel. Regarding to the distribution, hybridization and the presence of silica network into the CH matrix, similar results are reported in the literature [72], [73].

4.5. FTIR

The chemical structure of the hybrid composite and its parent constituents were examined using FTIR. The FTIR spectra of hybrid chitosan/silica, chitosan Hand TEOS are shown in Figure 24. The main absorption bands of CH-MA at 1640, 1540 and 1490 cm^{-1} could be assigned to the C=O stretching of amide I band, N-H bending (Amide II) and C-H bending of CH_2, respectively. Other absorption bands are 1373, 1317 cm^{-1} which can relate to CH_3 symmetrical deformation and C-N stretching of amide III, and 1635 and 815 cm^{-1} which are due to the C=O double bands due to methacrylation [74],[75].

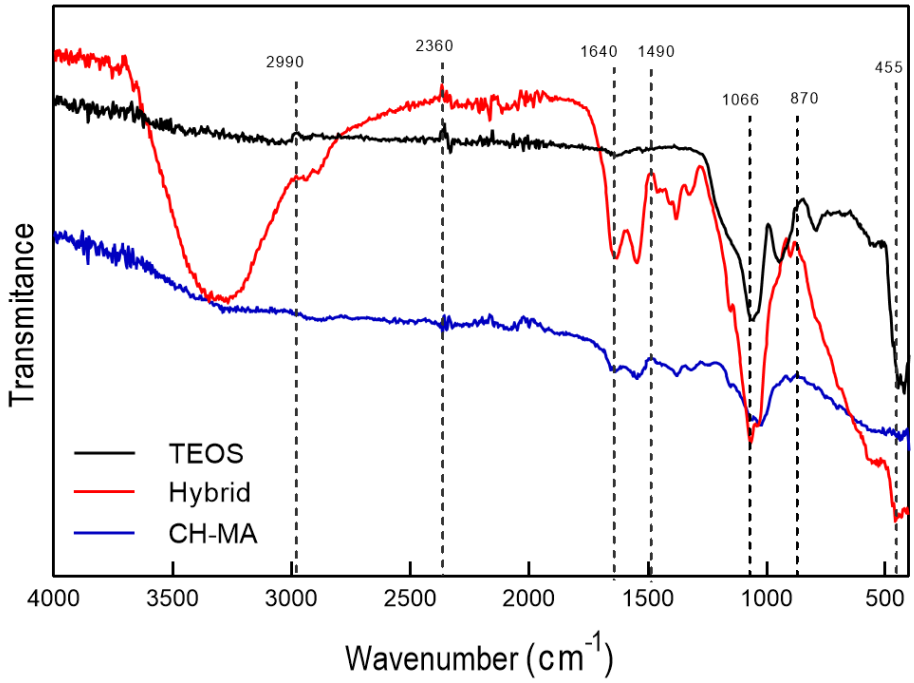

Figure 24. ATR-FTIR spectra of TEOS, Hybrid and CH-MA scaffolds.

The intense peak located at 3310 cm^{-1} in the hybrid is characteristic of water and ethanol, thus showing its presence in the sample. The formation of siloxane linkage from polycondensation in the hybrid was confirmed by the characteristic bands at 1066, 870 and 455 cm^{-1} corresponding to the asymmetric stretching, symmetric stretching and symmetric bending of the Si−O−Si, respectively, and the peak at 1066 cm^{-1} also corresponds to bonding interaction between CH_2−OH of chitosan [76],[77]. In general, these observations confirm the formation of hybrid chitosan/silica composite.

4.6. TGA

To study the thermal decomposition of hybrid, thermogravimetric analysis was performed under a nitrogen atmosphere at the temperature ranging from 30ºC – 800ºC (Figure 25).

The losses that occurred up to 100°C in all materials were due to water loss from the scaffolds. CH exhibits a highly hydrophilic behavior [78] due to the hydroxyl and amino groups and the complete removal of water is difficult [79]. Furthermore, silica produced by sol-gel is also hydrophilic due to free silanol groups (Si-OH) that are present in its surface [80]. The thermal degradation of the organic material, CH, occurred mostly around 360ºC due to the complex dehydration of depolymerization, saccharide rings and species with low molecular weight [81]. In the case where silica is combined with the polymer in the hybrid, the resistance of the material to thermal decomposition was considerably improved and, by observing Figure 25, one could conclude that the hybrid would have lost 60% of its initial weight. However, there are some aspects to be taken into account, such as the fact that up to 400ºC in the case of TEOS, 27% of the initial mass was lost, losses that consisted mostly of water, ethanol and acid that make up the sample. Therefore, and knowing that the hybrid has present in its constitution the same TEOS solution, when analyzing the decomposition of the hybrid it must be considered that 27% of the initial loss is due to the above explained and, therefore, disregard the 27% of initial weight loss of the hybrid that corresponds to the temperature of 240ºC. The mass of material remaining at 800°C of the hybrid is higher than the chitosan, represented with 38.4% compared to 12% of CH and the remaining mass in the hybrid corresponds to the amount of silica integrated into the hybrid.

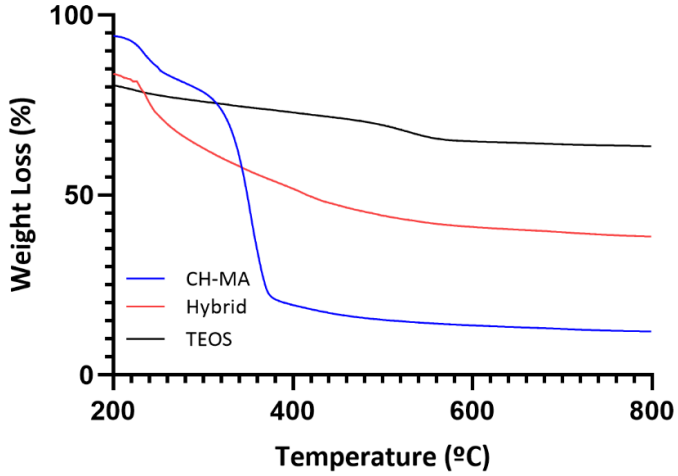

Figure 25. TGA curves of CH-MA, Hybrid and TEOS.

The sample used that comes closest to pure silica is the one denominated TEOS, where the TEOS solution was allowed to condense completely and then dried at RT. If pure silica had been used, one would not expect to see a decomposition curve since an inorganic material does not burn easily [82], but since the sample used was the TEOS solution described in the previous section, the losses up to 400°C were mainly due to the removal of water, solvent residues, and volatile compounds. However, and as expected, the mass remaining in this sample was much higher than the hybrid and the organic compound, accounting for 65%, proving that silica has excellent thermal properties and

thus restraint from decomposing at high temperatures [83]. These results are in line with expectations, based on some previously reported studies [58],[82].

4.7. Cytotoxicity profile

To evaluate the cytotoxicity profile of the scaffolds, cell viability assays were performed: an MTS assay was carried out to quantify the metabolic activity of L929 mouse fibroblasts and a live/dead kit assay to observe the viable cells in contact with the different materials, for 1 and 7 days.

4.7.1. MTS

The cell metabolic activity of cultured L929 was quantified by MTS colorimetric assay at days 1 and 7 of culture (Figure 26). The MTS assay shows that the materials do not elicit any cytotoxic response for 7 days. When comparing the hybrid material with the CH, both have similar biocompatible profiles after 7 days in in contact with L929 cell line. This study is in accordance with others reported in literature where hybrids composed of TEOS and CH-MA do not show any cytotoxicity [84], [85].

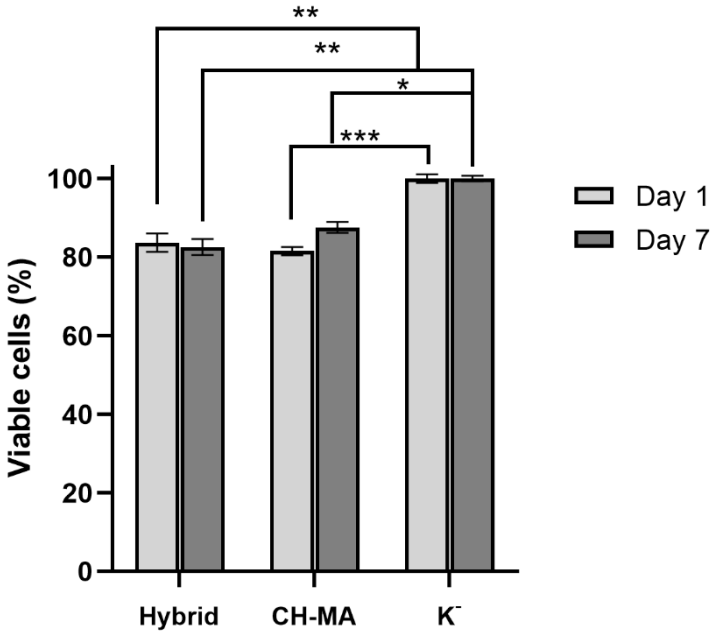

Figure 26. MTS viability assay at 1 and 7 days of culture - hybrid and CH-MA scaffolds with L929 mouse fibroblasts cells. Statistically differences are marked with (*), (**) and (***) which stand for $p < 0.05$, $p < 0.01$ and $p < 0.001$, respectively.

4.7.2. Live/Dead assay – Cell viability

L929 mouse fibroblasts were used to evaluate the cytotoxicity profile of hybrid and CH-MA scaffolds through live/dead assays. After 24h of incubation at 37ºC, cell viability was analyzed by image acquisition. On day 1, although the toxicity profile of the materials under study did not match that of control, they were shown to be viable. As shown in the Figure 27, L929 cells are found around the two types of scaffolds and the dead cells is almost non-existent.

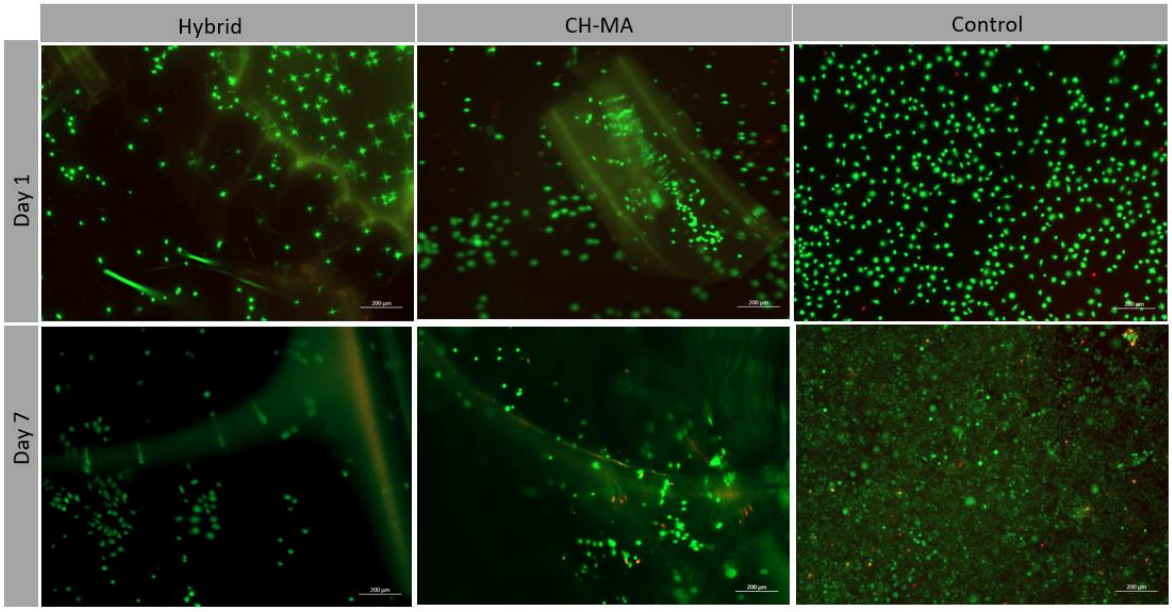

Figure 27. Fluorescence images (5x) of L929 mouse fibroblast cells stained with Calcein and PI in contact with hybrid and CH-MA scaffolds.

In case of CH-MA scaffold, from day 1 to day 7, there are already more dead cells compared to that of the hybrid structure, although it does not seem to be very significant. After 7 days of the L929 cells being incubated at 37ºC with the scaffolds, there was not a significant decrease in cell viability in both scaffolds compared to the day 1. When comparing with the control, the hybrid and CH-MA scaffolds presents much less cells. These results are in agreement with those obtained in MTS assay discussed before and allows to conclude that both scaffolds are not cytotoxic to cells. Moreover, the absence of cells after 7 days either on CH-MA or the hybrid can be attributed to the inexistence of cell adhesion motifs on their composition, as reported by other studies [86],[87],[88]. However, to conclude about cellular viability, a DNA quantification assay is needed. These cell viability results are in line with others reported in the literature using the same materials [85], [86].

4.8. Biomineralization activity in SBF

Bone regeneration ability of a bioactive material is related with the formation of hydroxyapatite ($Ca_{10}(PO_4)_6(OH)_2$) layer which is a resemblance to human bone. Biomineralization study has been applied to evaluate the bone regeneration capability from the relationship between the apatite formation *in vitro* and the ability to promote bone growth and regeneration *in vivo* [62]. Bioactive scaffolds with a mean curvature of zero that resembles the mean curvature of trabecular bone are of great interest in this aspect.

In this assay, the methacrylated CH and hybrid were evaluated for their in vitro apatite forming ability in simulated body fluid. After 14 and 21 days of the test, surface morphology and elemental composition of the scaffolds were observed by SEM-EDS. From the SEM images (Figure 28), the CH-MA scaffold did not exhibit any sign of apatite formation throughout the entire teste, indicating a poor bioactivity, which is in line with reported in the literature using CH-MA [89]. The hybrid scaffolds on 21st day shows some salts formation in its surface but could not be detected apatite crystals. Analyzing the table in Figure 28, where the elemental composition of the surface of the hybrid scaffolds is represented, it is clear that amount of calcium and phosphate increase from 14 to 21 days, and the silica decrease throughout these days.

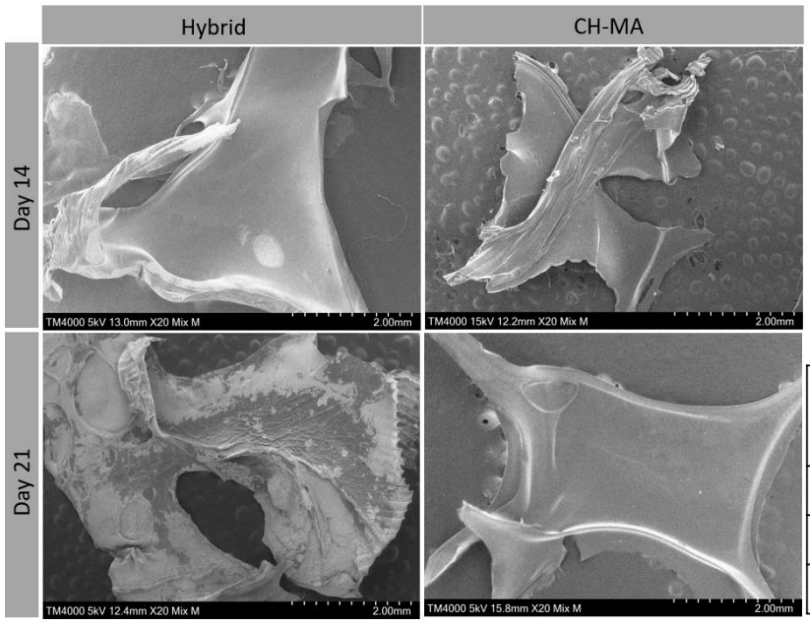

Element	At %	
	Day 14	Day 21
Si	50.30	9.91
Ca	39.46	68.31
P	10.25	21.78

Figure 28. SEM images of the chitosan Hand the hybrid scaffolds (left) and elemental composition of surface of the hybrid scaffolds (right) after immersion in simulated body fluid for 14 and 21 days.

The emergence of salts in the hybrid surface at day 21 of assay can be related to the formation of an amorphous calcium-phosphate layer because, besides being in agreement with the elementary composition represented in Figure 28 (right), it is reported in the literature that depending on the amount of silica there may be no formation of hydroxyapatite crystals after 1 month of immersion in SBF, although the formation of an amorphous calcium-phosphate layer is observed [90], [91].

This assay would have to be repeated to reach a more assertive conclusion about amorphous calcium-phosphate layer formation, but it was not possible due to time issues.

5. General Conclusions and Future Perspectives

Regenerative medicine is a research field with a lot of potential for improving the quality of life of the patients by the versatility of allowing the combination of different biomaterials, techniques, and several strategies to develop scaffolds. Currently, the number of clinically approved therapies using biomaterials for Tissue Engineering is increasing but the effectiveness of these applications remains low.

Among the various organic-inorganic hybrid materials, CH and silica are two of the most studied materials, either in combination or individually. The CH has the advantage of its available functional groups that allows chemical modification, thus allowing certain features to be manipulated depending on the desired application. Silica, an inorganic compound, which can be obtained from some precursors such as TEOS via sol-gel chemistry, provides good mechanical and bioactive properties, and a better thermal resistance compared to polymers. In this work, a novel approach to construct a minimalistic organic-inorganic hybrid scaffold based on minimal surfaces of two geometries was developed where the synthesis and processing are not expensive. Through the study of elemental composition, TGA and FTIR we're able to conclude that the inorganic part was successfully incorporated into the organic one and that the introduction of an inorganic phase into the organic one improved the resistance to thermal decomposition of material. However, in the study of biomineralization in SBF, one would expect apatite crystals to form on the hybrid scaffold, but they were not detected on both scaffolds. The cytotoxicity profile of both materials was evaluated through biological assays – MTS and Live/Dead throughout 7 days and the results showed that hybrid and CH-MA scaffolds are not cytotoxic to L929 mouse fibroblasts cells.

The main shortcoming of this work is the fact that a 3D interconnected scaffold was not obtained, so this is the main aspect in the future work to be done – a minimal surface 3D scaffold. Then, the need to increase the amount of inorganic compound without compromising the final structure has to be overcome and, with this, study the effect this increase has on the mechanical and bioactive properties of the scaffold. Another future work is to evaluate the adherence and behavior of osteoblast cells in contact to 3D hybrid scaffolds, having in mind the mean bone curvature and to expand this study to other geometries depending on the application of the minimal surface structures.

6. Bibliography

[1] K. Lee, E. A. Silva, and D. J. Mooney, "Growth factor delivery-based tissue engineering: General approaches and a review of recent developments," *J. R. Soc. Interface*, vol. 8, no. 55, pp. 153–170, 2011, doi: 10.1098/rsif.2010.0223.

[2] N. Iqbal, A. S. Khan, A. Asif, M. Yar, J. W. Haycock, and I. U. Rehman, "Recent concepts in biodegradable polymers for tissue engineering paradigms: a critical review," *Int. Mater. Rev.*, vol. 64, no. 2, pp. 91–126, Feb. 2019, doi: 10.1080/09506608.2018.1460943.

[3] N. Goonoo and A. Bhaw-Luximon, "Mimicking growth factors: role of small molecule scaffold additives in promoting tissue regeneration and repair," *RSC Adv.*, vol. 9, no. 32, pp. 18124–18146, 2019, doi: 10.1039/C9RA02765C.

[4] S. Safinsha and M. Mubarak Ali, "Composite scaffolds in tissue engineering," *Mater. Today Proc.*, vol. 24, pp. 2318–2329, 2019, doi: 10.1016/j.matpr.2020.03.761.

[5] C. Murphy, F. O'Brien, D. Little, and A. Schindeler, "Cell-scaffold interactions in the bone tissue engineering triad," *Eur. Cells Mater.*, vol. 26, pp. 120–132, Sep. 2013, doi: 10.22203/eCM.v026a09.

[6] Y. Kang, E. Jabbari, and Y. Yang, "Integration top-down and bottom-up scaffolding tissue engineering approach for bone regeneration," in *Micro and Nanotechnologies in Engineering Stem Cells and Tissues*, South Carolina: The Institute of Electrical and Electronics Engineers, 2013, pp. 142–158.

[7] F. Rey *et al.*, "Advances in Tissue Engineering and Innovative Fabrication Techniques for 3-D-Structures: Translational Applications in Neurodegenerative Diseases," *Cells*, vol. 9, no. 7, p. 1636, Jul. 2020, doi: 10.3390/cells9071636.

[8] J. W. Nichol and A. Khademhosseini, "Modular tissue engineering: engineering biological tissues from the bottom up," *Soft Matter*, vol. 5, no. 7, p. 1312, 2009, doi: 10.1039/b814285h.

[9] A. Aravamudhan *et al.*, "Osteoinductive Small Molecules: Growth Factor Alternatives for Bone Tissue Engineering," *Curr. Pharm. Des.*, vol. 19, no. 19, pp. 3420–3428, 2013, doi: 10.2174/1381612811319190008.

[10] A. A. Zadpoor, "Bone tissue regeneration: The role of scaffold geometry," *Biomater. Sci.*, vol. 3, no. 2, pp. 231–245, 2015, doi: 10.1039/c4bm00291a.

[11] S. Vijayavenkataraman, L. Zhang, S. Zhang, J. Y. H. Fuh, and W. F. Lu, "Triply periodic minimal surfaces sheet scaffolds for tissue engineering applications: An optimization approach toward biomimetic scaffold design," *ACS Appl. Bio Mater.*, vol. 1, no. 2, pp. 259–269, 2018, doi: 10.1021/acsabm.8b00052.

[12] I. Blei, "The science of soap films and soap bubbles (Isenberg, Cyril, ed.)," *J. Chem. Educ.*, vol. 58, no. 5, p. A179, May 1981, doi: 10.1021/ed058pA179.1.

[13] D. Lovett and C. Van Siclen, "Demonstrating Science with Soap Films," *Am. J. Phys.*, vol. 63, no. 9, pp. 860–861, Sep. 1995, doi: 10.1119/1.17817.

[14] S. C. Kapfer, S. T. Hyde, K. Mecke, C. H. Arns, and G. E. Schröder-Turk, "Minimal surface scaffold designs for tissue engineering," *Biomaterials*, vol. 32, no. 29, pp. 6875–6882, 2011, doi: 10.1016/j.biomaterials.2011.06.012.

[15] G. E. Schröder-turk *et al.*, “The chiral structure of porous chitin within the wing-scales of Callophrys rubi,” *J. Struct. Biol.*, vol. 174, pp. 290–295, 2011, doi: 10.1016/j.jsb.2011.01.004.

[16] J. W. Galusha, L. R. Richey, J. S. Gardner, J. N. Cha, and M. H. Bartl, “Discovery of a diamond-based photonic crystal structure in beetle scales,” *Phys. Rev. E*, vol. 77, no. 5, p. 050904, May 2008, doi: 10.1103/PhysRevE.77.050904.

[17] Y. Feng and J. Guo, “Biodegradable Polydepsipeptides,” *Int. J. Mol. Sci.*, vol. 10, no. 2, pp. 589–615, Feb. 2009, doi: 10.3390/ijms10020589.

[18] S. Bhatia, *Natural Polymer Drug Delivery Systems*. Cham: Springer International Publishing, 2016.

[19] T. Kean and M. Thanou, “Chapter 10. Chitin and Chitosan: Sources, Production and Medical Applications,” in *Renewable Resources for Functional Polymers and Biomaterials: Polysaccharides, Proteins and Polyesters*, Cambridge, England: Royal Society of Chemistry, 2011, pp. 292–318.

[20] K. Takai, T. Ohtsuka, Y. Senda, M. Nakao, and K. Yamamoto, “Antibacterial Properties of Antimicrobial-Finished Textile Products,” *Microbiol. Immunol.*, vol. 46, no. 2, pp. 75–81, 2002.

[21] G. A. El-mahdy, A. M. Atta, H. A. Al-lohedan, and A. O. Ezzat, “Influence of Green Corrosion Inhibitor based on Chitosan Ionic Liquid on the Steel Corrodibility in Chloride Solution,” *Int. J. Eletrochemical Sci.*, vol. 10, pp. 5812–5826, 2015.

[22] A. K. Gaharwar, S. A. Dammu, J. M. Canter, C. Wu, and G. Schmidt, “Highly Extensible, Tough, and Elastomeric Nanocomposite Hydrogels from Poly(ethylene glycol) and Hydroxyapatite Nanoparticles,” *Biomacromolecules*, vol. 12, no. 5, pp. 1641–1650, May 2011, doi: 10.1021/bm200027z.

[23] A. Hafidh, F. Touati, and F. Sediri, “Synthesis, charaterization and optical properties of nanostructured silica hybrid materials obtained by soft chemistry from perhydropolysilazane/1,2,4-triazole precursors,” *J. Mol. Struct.*, vol. 1218, 2020, doi: 10.1016/j.molstruc.2020.128496.

[24] S. C. Daminabo, S. Goel, S. A. Grammatikos, H. Y. Nezhad, and V. K. Thakur, “Fused deposition modeling-based additive manufacturing (3D printing): techniques for polymer material systems,” *Mater. Today Chem.*, vol. 16, p. 100248, Jun. 2020, doi: 10.1016/j.mtchem.2020.100248.

[25] S. Bose, S. Vahabzadeh, and A. Bandyopadhyay, “Bone tissue engineering using 3D printing,” *Mater. Today*, vol. 16, no. 12, pp. 496–504, Dec. 2013, doi: 10.1016/j.mattod.2013.11.017.

[26] R. Schmelzeisen and M. Rolf, “Rapid prototyping of scaffolds derived from thermoreversible hydrogels and tailored for applications in tissue engineering,” *Biomaterials*, vol. 23, pp. 4437–4447, 2002.

[27] K. Bryll, E. Piesowicz, P. Szymański, W. Ślączka, and M. Pijanowski, “Polymer Composite Manufacturing by FDM 3D Printing Technology,” *MATEC Web Conf.*, vol. 237, p. 02006, Nov. 2018, doi: 10.1051/matecconf/201823702006.

[28] S. C. Ligon, R. Liska, J. Stampfl, M. Gurr, and R. Mülhaupt, “Polymers for 3D Printing and Customized Additive Manufacturing,” *Chem. Rev.*, vol. 117, no. 15, pp. 10212–10290, Aug. 2017, doi: 10.1021/acs.chemrev.7b00074.

[29] M. S. Lord, M. Foss, and F. Besenbacher, “Influence of nanoscale surface topography on protein adsorption and cellular response,” *Nano Today*, vol. 5, no. 1, pp. 66–78, Feb. 2010, doi: 10.1016/j.nantod.2010.01.001.

[30] V. Karageorgiou and D. Kaplan, “Porosity of 3D biomaterial scaffolds and osteogenesis,” *Biomaterials*, vol. 26, no. 27, pp. 5474–5491, Sep. 2005, doi: 10.1016/j.biomaterials.2005.02.002.

[31] C. M. Bidan *et al.*, “How Linear Tension Converts to Curvature: Geometric Control of Bone Tissue Growth,” *PLoS One*, vol. 7, no. 5, p. e36336, May 2012, doi: 10.1371/journal.pone.0036336.

[32] M. Rumpler, A. Woesz, J. W. C. Dunlop, J. T. van Dongen, and P. Fratzl, “The effect of geometry on three-dimensional tissue growth,” *J. R. Soc. Interface*, vol. 5, no. 27, pp. 1173–1180, Oct. 2008, doi: 10.1098/rsif.2008.0064.

[33] E. Gamsjäger, C. M. Bidan, F. D. Fischer, P. Fratzl, and J. W. C. Dunlop, “Modelling the role of surface stress on the kinetics of tissue growth in confined geometries,” *Acta Biomater.*, vol. 9, no. 3, pp. 5531–5543, Mar. 2013, doi: 10.1016/j.actbio.2012.10.020.

[34] G. Campoli, M. S. Borleffs, S. Amin Yavari, R. Wauthle, H. Weinans, and A. A. Zadpoor, “Mechanical properties of open-cell metallic biomaterials manufactured using additive manufacturing,” *Mater. Des.*, vol. 49, pp. 957–965, Aug. 2013, doi: 10.1016/j.matdes.2013.01.071.

[35] J. A. Sanz-Herrera, P. Moreo, J. M. García-Aznar, and M. Doblaré, “On the effect of substrate curvature on cell mechanics,” *Biomaterials*, vol. 30, no. 34, pp. 6674–6686, Dec. 2009, doi: 10.1016/j.biomaterials.2009.08.053.

[36] C. M. Bidan, F. M. Wang, and J. W. C. Dunlop, “A three-dimensional model for tissue deposition on complex surfaces,” *Comput. Methods Biomech. Biomed. Engin.*, vol. 16, no. 10, pp. 1056–1070, Oct. 2013, doi: 10.1080/10255842.2013.774384.

[37] S. Vijayavenkataraman, L. Y. Kuan, and W. F. Lu, “3D-printed ceramic triply periodic minimal surface structures for design of functionally graded bone implants,” *Mater. Des.*, vol. 191, p. 108602, Jun. 2020, doi: 10.1016/j.matdes.2020.108602.

[38] H. Jinnai, H. Watashiba, T. Kajihara, Y. Nishikawa, M. Takahashi, and M. Ito, “Surface curvatures of trabecular bone microarchitecture,” *Bone*, vol. 30, no. 1, pp. 191–194, Jan. 2002, doi: 10.1016/S8756-3282(01)00672-X.

[39] S. B. G. Blanquer *et al.*, “Surface curvature in triply-periodic minimal surface architectures as a distinct design parameter in preparing advanced tissue engineering scaffolds,” *Biofabrication*, vol. 9, no. 2, p. 025001, Apr. 2017, doi: 10.1088/1758-5090/aa6553.

[40] G. C. Shearman, O. Ces, R. H. Templer, and J. M. Seddon, “Inverse lyotropic phases of lipids and membrane curvature,” *J. Phys. Condens. Matter*, vol. 18, no. 28, pp. S1105–S1124, Jul. 2006, doi: 10.1088/0953-8984/18/28/S01.

[41] B. Tenchov and R. Koynova, “Cubic phases in membrane lipids,” *Eur. Biophys. J.*, vol. 41, no. 10, pp. 841–850, Oct. 2012, doi: 10.1007/s00249-012-0819-3.

[42] J. C. Eriksson and S. Ljunggren, “The Mechanical Surface Tension and Stability of Minimal Surface Structures,” *J. Colloid Interface Sci.*, vol. 167, no. 2, pp. 227–231, Oct. 1994, doi: 10.1006/jcis.1994.1356.

[43] P. J. F. Gandy, S. Bardhan, A. L. Mackay, and J. Klinowski, “Nodal surface approximations to the P,G,D and I-WP triply periodic minimal surfaces,” *Chem. Phys. Lett.*, vol. 336, no. 3–4, pp. 187–195, Mar. 2001, doi: 10.1016/S0009-2614(00)01418-4.

[44] J. E. Taylor, “Soap bubbles and crystals,” *Resonance*, vol. 11, no. 6, pp. 26–30, Jun. 2006, doi: 10.1007/BF02838879.

[45] F. J. Almgren and J. E. Taylor, “The Geometry of Soap Films and Soap Bubbles,” *Sci. Am.*, vol. 235, no. 1, pp. 82–93, Jul. 1976, doi: 10.1038/scientificamerican0776-82.

[46] W. H. Meeks and G. Tinaglia, “Triply periodic constant mean curvature surfaces,” *Adv. Math. (N. Y).*, vol. 335, no. March, pp. 809–837, Sep. 2018, doi: 10.1016/j.aim.2018.07.018.

[47] Y.-H. Han, A. Taylor, M. D. Mantle, and K. M. Knowles, “Sol–gel-derived organic–inorganic hybrid materials,” *J. Non. Cryst. Solids*, vol. 353, no. 3, pp. 313–320, Mar. 2007, doi: 10.1016/j.jnoncrysol.2006.05.042.

[48] G. Philipp and H. Schmidt, “New materials for contact lenses prepared from Si- and Ti-alkoxides by the sol-gel process,” *J. Non. Cryst. Solids*, vol. 63, no. 1–2, pp. 283–292, Feb. 1984, doi: 10.1016/0022-3093(84)90407-1.

[49] Y. Shirosaki, Y. Nakamura, T. Yoshioka, and A. Osaka, “Inorganic-Organic Hybrids for Biomedical Applications,” in *Handbook of Sol-Gel Science and Technology*, Cham: Springer International Publishing, 2018, pp. 3619–3703.

[50] G. J. Owens *et al.*, “Sol–gel based materials for biomedical applications,” *Prog. Mater. Sci.*, vol. 77, pp. 1–79, Apr. 2016, doi: 10.1016/j.pmatsci.2015.12.001.

[51] F. Al-Sagheer and S. Muslim, “Thermal and Mechanical Properties of Chitosan/ SiO2 Hybrid Composites,” *J. Nanomater.*, vol. 2010, pp. 1–7, 2010, doi: 10.1155/2010/490679.

[52] M. M. Seraji, G. Sameri, J. Davarpanah, and A. R. Bahramian, “The effect of high temperature sol-gel polymerization parameters on the microstructure and properties of hydrophobic phenol-formaldehyde/silica hybrid aerogels,” *J. Colloid Interface Sci.*, vol. 493, pp. 103–110, May 2017, doi: 10.1016/j.jcis.2017.01.014.

[53] S.-M. Lai, A. J.-M. Yang, W.-C. Chen, and J.-F. Hsiao, “The Properties and Preparation of Chitosan/Silica Hybrids Using Sol-Gel Process,” *Polym. Plast. Technol. Eng.*, vol. 45, no. 9, pp. 997–1003, Sep. 2006, doi: 10.1080/03602550600726269.

[54] F. Qi, Z. Cai, X. Zhu, S. Shang, and L. Pei, “Synthesis, Characterization, and Performance of a Novel Polymeric Cationic Surfactant Based on Low Molecular Weight Chitosan and 3-Chloro-2-Hydroxypropyl Dimethyl Dehydroabietyl Ammonium Chloride (CHPDMDHA),” *J. Surfactants Deterg.*, vol. 18, no. 3, pp. 463–470, May 2015, doi: 10.1007/s11743-015-1676-8.

[55] P. Johnson, A. Trybala, V. Starov, and V. J. Pinfield, “Effect of synthetic surfactants on the environment and the potential for substitution by biosurfactants,” *Adv. Colloid Interface Sci.*, vol. 288, p. 102340, Feb. 2021, doi: 10.1016/j.cis.2020.102340.

[56] S. De, S. Malik, A. Ghosh, R. Saha, and B. Saha, “A review on natural surfactants,” *RSC Adv.*, vol. 5, no. 81, pp. 65757–65767, 2015, doi: 10.1039/C5RA11101C.

[57] A. B. Moldes, L. Rodríguez-López, M. Rincón-Fontán, A. López-Prieto, X. Vecino, and J. M. Cruz, “Synthetic and Bio-Derived Surfactants Versus Microbial Biosurfactants in the

Cosmetic Industry: An Overview," *Int. J. Mol. Sci.*, vol. 22, no. 5, p. 2371, Feb. 2021, doi: 10.3390/ijms22052371.

[58] A. Salama and P. Hesemann, "New N-guanidinium chitosan/silica ionic microhybrids as efficient adsorbent for dye removal from waste water," *Int. J. Biol. Macromol.*, vol. 111, pp. 762–768, May 2018, doi: 10.1016/j.ijbiomac.2018.01.049.

[59] A. Salama and P. Hesemann, "Synthesis and characterization of N-guanidinium chitosan/silica ionic hybrids as templates for calcium phosphate mineralization," *Int. J. Biol. Macromol.*, vol. 147, pp. 276–283, Mar. 2020, doi: 10.1016/j.ijbiomac.2020.01.046.

[60] A. M. S. Costa and J. F. Mano, "Highly robust hydrogels via a fast, simple and cytocompatible dual crosslinking-based process," *Chem. Commun.*, vol. 51, no. 86, pp. 15673–15676, 2015, doi: 10.1039/C5CC05564D.

[61] H. Lee, M. Kim, Y. Yoon, and W. Park, "Fluorescent Property of Chitosan Oligomer and Its Application as a Metal Ion Sensor," *Mar. Drugs*, vol. 15, no. 4, p. 105, Apr. 2017, doi: 10.3390/md15040105.

[62] T. Kokubo and H. Takadama, "How useful is SBF in predicting in vivo bone bioactivity?," *Biomaterials*, vol. 27, no. 15, pp. 2907–2915, May 2006, doi: 10.1016/j.biomaterials.2006.01.017.

[63] L. Zhu and K. M. Bratlie, "pH sensitive methacrylated chitosan hydrogels with tunable physical and chemical properties," *Biochem. Eng. J.*, vol. 132, pp. 38–46, Apr. 2018, doi: 10.1016/j.bej.2017.12.012.

[64] L. M. Y. Yu, K. Kazazian, and M. S. Shoichet, "Peptide surface modification of methacrylamide chitosan for neural tissue engineering applications," *J. Biomed. Mater. Res. Part A*, vol. 82A, no. 1, pp. 243–255, Jul. 2007, doi: 10.1002/jbm.a.31069.

[65] T. Ikeda *et al.*, "Fabrication and Characteristics of Chitosan Sponge as a Tissue Engineering Scaffold," *Biomed Res. Int.*, vol. 2014, pp. 1–8, 2014, doi: 10.1155/2014/786892.

[66] D. M. Anderson, S. M. Gruner, and S. Leibler, "Geometrical aspects of the frustration in the cubic phases of lyotropic liquid crystals.," *Proc. Natl. Acad. Sci.*, vol. 85, no. 15, pp. 5364–5368, Aug. 1988, doi: 10.1073/pnas.85.15.5364.

[67] T. Oka, N. Ohta, and S. T. Hyde, "Polar–Nonpolar Interfaces of Normal Bicontinuous Cubic Phases in Nonionic Surfactant/Water Systems Are Parallel to the Gyroid Surface," *Langmuir*, vol. 36, no. 30, pp. 8687–8694, Aug. 2020, doi: 10.1021/acs.langmuir.0c00597.

[68] A. Pavan, H. S. Hoffmann, and Y. Gushikem, "The gelation temperature effects in the anilinepropylsilica xerogel properties," *Mater. Lett.*, vol. 55, pp. 378–382, 2002.

[69] C. J. Brinker and P. R. Schunk, "Hydrolysis and Condensation II:Silicates," in *Sol-Gel Science: The physics and Chemistry of Sol-Gel Processing*, 1990, pp. 95–233.

[70] W. A. A. Twej, "Temperature influence on the gelation process of tetraethylorthosilicate using sol-gel technique," *Iraqi J. Sci.*, vol. 50, no. 1, pp. 43–49, 2009.

[71] W. Wei *et al.*, "Preparation and Application of Novel Microspheres Possessing Autofluorescent Properties," *Adv. Funct. Mater.*, vol. 17, no. 16, pp. 3153–3158, Nov. 2007, doi: 10.1002/adfm.200700274.

[72] I. A. Wonnie Ma *et al.*, "Preparation of Hybrid Chitosan/Silica Composites Via Ionotropic

Gelation and Its Electrochemical Impedance Studies," *Prog. Org. Coatings*, vol. 145, p. 105679, Aug. 2020, doi: 10.1016/j.porgcoat.2020.105679.

[73] E. Lee, D. Shin, H.-E. Kim, H. Kim, Y. Koh, and J. Jang, "Membrane of hybrid chitosan–silica xerogel for guided bone regeneration," *Biomaterials*, vol. 30, no. 5, pp. 743–750, Feb. 2009, doi: 10.1016/j.biomaterials.2008.10.025.

[74] G. Bayramoğlu, "Methacrylated Chitosan Based UV Curable Support for Enzyme Immobilization," *Mater. Res.*, vol. 20, no. 2, pp. 452–459, Feb. 2017, doi: 10.1590/1980-5373-mr-2016-0789.

[75] K. John Kasongo, D. J. Tubadi, L. D. Bampole, T. A. Kaniki, N. J. M. Kanda, and M. E. Lukumu, "Extraction and characterization of chitin and chitosan from Termitomyces titanicus," *SN Appl. Sci.*, vol. 2, no. 3, p. 406, Mar. 2020, doi: 10.1007/s42452-020-2186-5.

[76] F. Rubio, J. Rubio, and J. L. Oteo, "A FT-IR Study of the Hydrolysis of Tetraethylorthosilicate (TEOS).," *Spectrosc. Lett.*, vol. 31, no. 1, pp. 199–219, Jan. 1998, doi: 10.1080/00387019808006772.

[77] D. Wang *et al.*, "Effect of inorganic/organic ratio and chemical coupling on the performance of porous silica/chitosan hybrid scaffolds," *Mater. Sci. Eng. C*, vol. 70, pp. 969–975, Jan. 2017, doi: 10.1016/j.msec.2016.04.010.

[78] S. Ludwiczak and M. Mucha, "Modeling of water sorption isotherms of chitosan blends," *Carbohydr. Polym.*, vol. 79, no. 1, pp. 34–39, Jan. 2010, doi: 10.1016/j.carbpol.2009.07.014.

[79] M. T. Viciosa, M. Dionísio, and J. F. Mano, "Dielectric characterization of neutralized and nonneutralized chitosan upon drying," *Biopolymers*, vol. 81, no. 3, pp. 149–159, Feb. 2006, doi: 10.1002/bip.20378.

[80] A. Stathopoulos *et al.*, "Water sorption and polymer dynamics in hybrid poly(2-hydroxyethyl-co-ethyl acrylate)/silica hydrogels," *Eur. Polym. J.*, vol. 46, no. 1, pp. 101–111, Jan. 2010, doi: 10.1016/j.eurpolymj.2009.10.014.

[81] M. Ziegler-Borowska, D. Chełminiak, H. Kaczmarek, and A. Kaczmarek-Kędziera, "Effect of side substituents on thermal stability of the modified chitosan and its nanocomposites with magnetite," *J. Therm. Anal. Calorim.*, vol. 124, no. 3, pp. 1267–1280, Jun. 2016, doi: 10.1007/s10973-016-5260-x.

[82] I. A. Wonnie Ma, A. Sh., S. Bashir, S. S. A Kumar, R. K, and R. S, "Development of active barrier effect of hybrid chitosan/silica composite epoxy-based coating on mild steel surface," *Surfaces and Interfaces*, vol. 25, p. 101250, Aug. 2021, doi: 10.1016/j.surfin.2021.101250.

[83] J. Tan *et al.*, "Facile preparation of hybrid vesicles loaded with silica nanoparticles via aqueous photoinitiated polymerization-induced self-assembly," *RSC Adv.*, vol. 7, no. 37, pp. 23114–23121, 2017, doi: 10.1039/C7RA02770B.

[84] Z. Deng, Z. Zhen, X. Hu, S. Wu, Z. Xu, and P. K. Chu, "Hollow chitosan–silica nanospheres as pH-sensitive targeted delivery carriers in breast cancer therapy," *Biomaterials*, vol. 32, no. 21, pp. 4976–4986, Jul. 2011, doi: 10.1016/j.biomaterials.2011.03.050.

[85] Y. Dong, J. Liang, Y. Cui, S. Xu, and N. Zhao, "Fabrication of novel bioactive hydroxyapatite-chitosan-silica hybrid scaffolds: Combined the sol-gel method with 3D plotting technique," *Carbohydr. Polym.*, vol. 197, pp. 183–193, Oct. 2018, doi: 10.1016/j.carbpol.2018.05.086.

[86] A. Pipattanawarothai, C. Suksai, K. Srisook, and T. Trakulsujaritchok, “Non-cytotoxic hybrid bioscaffolds of chitosan-silica: Sol-gel synthesis, characterization and proposed application,” *Carbohydr. Polym.*, vol. 178, pp. 190–199, Dec. 2017, doi: 10.1016/j.carbpol.2017.09.047.

[87] J.-S. Oh and E.-J. Lee, “Engineered dressing of hybrid chitosan-silica for effective delivery of keratin growth factor and acceleration of wound healing,” *Mater. Sci. Eng. C*, vol. 103, p. 109815, Oct. 2019, doi: 10.1016/j.msec.2019.109815.

[88] S. Trujillo, E. Pérez-Román, A. Kyritsis, J. L. Gómez Ribelles, and C. Pandis, “Organic-inorganic bonding in chitosan-silica hybrid networks: Physical properties,” *J. Polym. Sci. Part B Polym. Phys.*, vol. 53, no. 19, pp. 1391–1400, Oct. 2015, doi: 10.1002/polb.23774.

[89] Z.-K. Cui, S. Kim, J. J. Baljon, B. M. Wu, T. Aghaloo, and M. Lee, “Microporous methacrylated glycol chitosan-montmorillonite nanocomposite hydrogel for bone tissue engineering,” *Nat. Commun.*, vol. 10, no. 1, p. 3523, Dec. 2019, doi: 10.1038/s41467-019-11511-3.

[90] J. Wilson, G. H. Pigott, F. J. Schoen, and L. L. Hench, “Toxicology and biocompatibility of bioglasses,” *J. Biomed. Mater. Res.*, vol. 15, no. 6, pp. 805–817, Nov. 1981, doi: 10.1002/jbm.820150605.

[91] F. Baino and S. Yamaguchi, “The Use of Simulated Body Fluid (SBF) for Assessing Materials Bioactivity in the Context of Tissue Engineering: Review and Challenges,” *Biomimetics*, vol. 5, no. 4, p. 57, Oct. 2020, doi: 10.3390/biomimetics5040057.